

RESEARCH ARTICLE

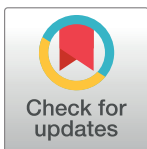
Loss of *Fnip1* alters kidney developmental transcriptional program and synergizes with *TSC1* loss to promote mTORC1 activation and renal cyst formation

Ryan Centini¹, Mark Tsang¹, Terri Iwata¹, Heon Park¹, Jeffrey Delrow², Daciana Margineantu³, Brandon M. Iritani¹, Haiwei Gu^{4*}, H. Denny Liggitt¹, Janella Kang¹, Lim Kang¹, David M. Hockenbery^{3,5}, Daniel Raftery^{4,5}, Brian M. Iritani^{1*}

1 The Department of Comparative Medicine, University of Washington, Seattle, Washington, United States of America, **2** Genomics and Bioinformatics Shared Resources, Fred Hutchinson Cancer Research Center, Seattle, Washington, United States of America, **3** Clinical Division, Fred Hutchinson Cancer Research Center, Seattle, Washington, United States of America, **4** Department of Anesthesiology and Pain Medicine, Mitochondria and Metabolism Center, Northwest Metabolomics Research Center, University of Washington, Seattle, Washington, United States of America, **5** Public Health Sciences Division, Fred Hutchinson Cancer Research Center, Seattle, Washington, United States of America

* Current address: Center for Metabolic and Vascular Biology, School of Nutrition and Health Promotion, College of Health Solutions, Arizona State University, Phoenix, Arizona, United States of America

* biritani@uw.edu



OPEN ACCESS

Citation: Centini R, Tsang M, Iwata T, Park H, Delrow J, Margineantu D, et al. (2018) Loss of *Fnip1* alters kidney developmental transcriptional program and synergizes with *TSC1* loss to promote mTORC1 activation and renal cyst formation. *PLoS ONE* 13(6): e0197973. <https://doi.org/10.1371/journal.pone.0197973>

Editor: Niels Olsen Saraiva Câmara, Universidade de Sao Paulo, BRAZIL

Received: August 10, 2017

Accepted: May 13, 2018

Published: June 13, 2018

Copyright: © 2018 Centini et al. This is an open access article distributed under the terms of the [Creative Commons Attribution License](https://creativecommons.org/licenses/by/4.0/), which permits unrestricted use, distribution, and reproduction in any medium, provided the original author and source are credited.

Data Availability Statement: Data are freely available by contacting the senior author biritani@uw.edu. RNAseq data has been deposited in NIH Geo Omnibus (<https://www.ncbi.nlm.nih.gov/geo/>). For the GEO database files: a. Accession number GSE103303 b. Title: *Fnip1* null kidney versus wildtype kidney RNAseq data. This data comprises the minimal data set underlying our study.

Abstract

Birt-Hogg-Dube' Syndrome (BHDS) is a rare genetic disorder in humans characterized by skin hamartomas, lung cysts, pneumothorax, and increased risk of renal tumors. BHDS is caused by mutations in the *BHD* gene, which encodes for Folliculin, a cytoplasmic adapter protein that binds to Folliculin interacting proteins-1 and -2 (*Fnip1*, *Fnip2*) as well as the master energy sensor AMP kinase (AMPK). Whereas kidney-specific deletion of the *Bhd* gene in mice is known to result in polycystic kidney disease (PKD) and renal cell carcinoma, the roles of *Fnip1* in renal cell development and function are unclear. In this study, we utilized mice with constitutive deletion of the *Fnip1* gene to show that the loss of *Fnip1* is sufficient to result in renal cyst formation, which was characterized by decreased AMPK activation, increased mTOR activation, and metabolic hyperactivation. Using RNAseq, we found that *Fnip1* disruption resulted in many cellular and molecular changes previously implicated in the development of PKD in humans, including alterations in the expression of ion and amino acid transporters, increased cell adhesion, and increased inflammation. Loss of *Fnip1* synergized with *Tsc1* loss to hyperactivate mTOR, increase Erk activation, and greatly accelerate the development of PKD. Our results collectively define roles for *Fnip1* in regulating kidney development and function, and provide a model for how loss of *Fnip1* contributes to PKD and perhaps renal cell carcinoma.

Funding: This work was supported by the National Institutes of Health, RO1AI114556 (BI), R21AI10920 (BI, HP), R25OD010450 (BI), R56AI092093 (BI, HP). The funder had no role in study design, data collection and analysis, decision to publish, or preparation of the manuscript.

Competing interests: The authors have declared that no competing interests exist.

Introduction

Birt-Hogg-Dube' Syndrome (BHDS) is a rare autosomal dominant disorder in which affected individuals are at high risk of developing cutaneous fibrofolliculomas, bilateral pulmonary cysts, pneumothorax, and a variety of renal tumors including chromophobe renal cell carcinoma, clear cell renal carcinoma, oncocytoma, and papillary renal cell carcinoma (see [1, 2] for review). In 2002, BHDS was localized to germline mutations in the *BHD* gene, which encodes a tumor suppressor named Folliculin (FLCN)[3]. Additional protein-protein interaction studies revealed that the carboxy terminus of FLCN binds to two structurally related proteins called Folliculin interacting proteins-1 and -2 (FNIP1 and FNIP2), as well as the master metabolic regulator AMP kinase (AMPK)[4–6]. AMPK is an energy sensing molecule that is activated in response to low energy (low ATP/high AMP) via phosphorylation at threonine 172 by Liver Kinase B1 (LKB1) and by allosteric activation of AMPK upon AMP binding (see [7] for review). In some cell types such as T cells, AMPK is also phosphorylated and activated by Calmodulin-dependent protein Kinase Kinase (CaMKK) in response to calcium signals [8]. Once activated, AMPK stimulates energy production in part by stimulating mitochondrial biogenesis, fatty acid oxidation, glucose uptake, and autophagy, while also inhibiting energy and nutrient consumption by negatively regulating mechanistic target of rapamycin (mTOR). Specifically, AMPK phosphorylates and inhibits the essential mTOR co-activator Raptor[9], and phosphorylates and stimulates TSC2, a negative regulator of mTOR[10]. Whereas the exact roles of Folliculin in modulating these pathways are not clear, Folliculin/Fnip have been implicated in both inhibition and activation of AMPK[11–16], inhibition of mitochondrial biogenesis [17–19], inhibition and activation of autophagy[15, 20, 21], and inhibition and activation of mTOR [18, 22–26].

Constitutive deletion of the *Bhd* gene in mice results in early embryonic death[23]. Hence, the majority of *Flcn* studies in mice have involved either analyses of *Bhd* heterozygous mice, or conditional deletion of *Bhd* in a tissue specific manner using the Cre-LoxP system. Three independent research groups found that heterozygous *Bhd* (*Bhd*^{+/-}) mice developed PKD, which progressed to renal cancer with a median tumor-free survival of ~25 months [23, 26, 27]. Similar to BHDS, histological types of tumors from *Bhd*^{+/-} mice included oncocytic hybrid, oncocytoma, and clear cell tumors, which were characterized either by increased[23], decreased[26], or variable activation of mTOR depending on the tissue context[27]. Three additional studies whereby the *Bhd* gene was deleted in a kidney-specific manner in either distal[28, 29] or proximal tubules [30] of mice found that the mice initially developed PKD, which progressed to renal failure. These studies showed that loss of the *Bhd* gene resulted in pronounced upregulation of the AKT/mTOR signaling pathways and that treatment with the mTORC1 (mTORC1) inhibitor rapamycin could prevent the development of PKD. In a similar study, *Hasumi et al* conditionally deleted the *Bhd* gene in the proximal tubules using *CDH16*-Cre, and found that the development of PKD correlated with increased *Pgc1alpha* expression and increased mitochondrial metabolism. Disruption of the *Pgc1alpha* partially rescued the PDK phenotype in *Bhd* deficient mice[17]. Collectively, these studies suggest that disruption of Folliculin is sufficient to result in the development of PKD, and can in some cases progress to renal cancer due in part to increased activation of the mTOR pathway and increased mitochondrial biogenesis.

Although the roles and importance of Folliculin in kidney development and function have been extensively investigated, the roles of *Fnip1* and *Fnip2* in kidney development and function are not as clear. Recently, *Hasumi et al* generated *Fnip1*, *Fnip2* double knockout mice in a kidney specific manner[31]. The authors found no changes in the kidney development or function when either *Fnip1* or *Fnip2* were deleted alone, but when both genes were deleted together, the mice developed fatal PKD by 3 weeks of age. Interestingly, kidney specific

deletion of *Flcn* did not augment kidney size or cystic histology of *Fnip1*^{-/-}*Fnip2*^{-/-} double null kidneys, suggesting that *Fnip1/2* and *Flcn* likely act on convergent pathways. The authors also showed heterozygous *Fnip1*^{+/-}*Fnip2*^{-/-} mice developed hybrid oncocytic tumors at 24 months of age, similar to the tumor type found in BHDS patients.

In this study, we investigated the specific roles of *Fnip1* in renal development and function, using *Fnip1* null mice we previously generated using a random ENU mutagenesis strategy in mice [18]. In contrast to a previous report [31], we found that loss of *Fnip1* resulted in slightly enlarged kidney size and significantly increased renal cyst formation, which were characterized by decreased AMPK activation, focal increases in mTORC1 activation, and increased oxidative metabolism of renal epithelial cells. The local cyst environment exhibited increased immune cell infiltration, decreased expression of organic ion channels, and increased expression of cell adhesion molecules. Importantly, co-deletion of the mTORC1 inhibitor *Tsc1* with *Fnip1* resulted in greatly increased mTORC1 activation and accelerated PKD development relative to deletion of either gene alone.

Materials and methods

Mice

Fnip1^{-/-}, *Mb1-Cre*, *Tsc1*^{fl/fl} mice were developed as previously described [18, 32, 33]. Mice were housed under specific-pathogen-free conditions. *TSC1*^{fl/fl}*Mb1Cre*, *TSC1*^{fl/fl}*Mb1CreFnip1*^{+/-}, *TSC1*^{fl/fl}*Mb1CreFnip1*^{-/-} mice were humanely euthanized upon signs of compromised renal function. Rapamycin and control diets were milled at TestDiet (Richmond, IN) and impregnated with rapamycin (14ppm) in the lab of Dr. Randy Strong at the University of Texas Health Center, Barshop Institute (San Antonio, TX). For the *TSC1*^{fl/fl}*Mb1Cre* study, mice in the rapamycin treatment group were started on rapamycin chow after weaning and continued until euthanasia. All animal studies were reviewed and approved by the Institutional Animal Care and Use Committee of the University of Washington. Mice were humanely euthanized via CO₂ overdose according to the AVMA guidelines on euthanasia.

Immunoblotting

Tissue for immunoblotting and RNA analyses were flash frozen and stored at -80 degrees Celsius until lysis. Frozen kidneys were homogenized in RIPA buffer (Thermo Scientific Rockford, IL) with Halt Protease and Phosphatase Inhibitor™ (Thermo Scientific Rockford, IL). Protein concentrations were determined via the Micro BCA™ Protein Assay Kit (Thermo Scientific, Rockford, IL). Immunoblotting was performed as previously described [18, 34]. Blots were incubated overnight in primary antibodies obtained from Cell Signaling Technology (Danvers, MA), followed by incubation with horseradish peroxidase-conjugated secondary antibody. Antibodies used were: pERK(D13.14.4E; Rabbit mAb; Cat# 4370), Erk (137F5; Rabbit mAb; Cat#4695), p-AMPK (40H9; Rabbit mAb; Cat#2535), AMPK (Rabbit Ab; Cat#2532), pmTOR (D9C2; Rabbit mAb; Cat#5536), pS6R(D68F8; Rabbit mAb; Cat#5364), p4E-BP (235B4; Rabbit IgG; Cat#2855), 4E-BP(53H11; Rabbit mAb; Cat#9644), pAkt473 (D9E; Rabbit mAb; Cat#4060), pAkt308(D25E6; Rabbit mAb; Cat#13038), Actin (D6A8; Rabbit mAb; Cat#8457).

Histochemistry and immunohistochemistry

Kidneys were collected and fixed in 10% formalin. All special staining was performed at the University of Washington's Histology and Imaging Core (HIC). Phospho-S6R (Cell Signaling Technology, Danvers, MA), and F4/80 (Thermo Scientific, Waltham, MA), and anti-CD3epsilon (eBioscience, San Diego CA) antibodies were used. To count cysts, one kidney from 12–16

week-old male mice was fixed in 10% neutral buffered formalin and processed as previously described followed by staining with hematoxylin and eosin [29]. Sagittal sections of equivalent depth and orientation were evaluated by a board-certified veterinary pathologist. Cysts (> 5 x normal tubule diameter) and microcysts (<5X normal tubule diameter) were defined as translucent regions lined by renal tubular epithelial cells with blebs extending into the lumen. Cysts were counted by an individual blinded to the genotypes.

Quantitative PCR

RNA was purified from frozen kidney tissue with the use of RNeasy Mini Kit (Qiagen Valencia, CA). cDNA was synthesized from RNA via Invitrogen SuperScript II Reverse Transcriptase (Life Technologies Grand Island, NY). Gene-specific oligonucleotide primer sequences are listed in S4 Table. PCR reactions were performed using the SYBR green system as previously described[35]. For real-time quantitative PCR, differences were calculated using the comparative C_T method ($n = 3/\text{group}$)[36].

Seahorse assays

Renal tubular epithelial cells (TECs) were isolated from kidneys collected from 3 *Fnip1*^{-/-} and 3 *Fnip1*^{+/-} (wildtype) mice. Briefly, kidneys were dissected into 4 mls ice-cold Dulbecco's phosphate buffered saline (DPBS) (Gibco Grand Island, NY) and minced into pieces of ~ 1 mm³. Fragments were then transferred to collagenase solution (1 mg/ml in DPBS; Sigma-Aldrich St. Louis, MO) and digested for 60 minutes at 37 °C. The pellet was washed twice with DPBS before plating in 10 cm dishes to a confluence of 80–90%. Cells were cultured in RPMI media (Gibco, Grand Island, NY), 10% FBS, 100 units/ml penicillin G, 100 µg/ml streptomycin, and 20 ng/ml epidermal growth factor (Sigma-Aldrich St. Louis, MO). Cells were seeded on an XF96 microplate (Seahorse Biosciences) and incubated at 37 degrees Celsius for 6–12 hours prior to analysis. Cells were plated in DMEM +10mM glucose, 2mM glutamine, and 1mM pyruvate. Mitochondrial function was analyzed in accordance with the XF Cell Mito Stress Test Kit (Seahorse Biosciences) and basal respiratory and glycolytic rates were determined. Following basal measurements, cells were treated with oligomycin (2.5 µM), carbonyl cyanide 4-(trifluoromethoxy) phenylhydrazone (FCCP, 0.5 µM; Sigma C2920) and Antimycin (2 µM), rotenone (2 µM).

Metabolomics

Mass spectrometry experiments were performed in the Northwest Metabolomics Research Center at the University of Washington, using the broad-based LC-MS/MS approach[37–40]. 5–8 mg samples of frozen kidney was collected from age and matched *Fnip1*^{-/-} and *Fnip1*^{+/-} control mice were homogenized in 50% methanol at -80 °C ($n = 4/\text{group}$). Results were normalized based on tissue weight. Mass spectrometry was performed as previously described [12]. Data were analyzed using MetaboAnalyst 3.0. Partial Least Squares-Discriminant Analysis (PLS-DA), which uses multivariate regression techniques to extract linear combination of variables, was utilized to establish differences. Variable Importance in Projection (VIP) is the weighted sum of squares of the PLS loadings taking into account the amount of explained Y-variation in each dimension[41].

RNAseq

RNA was purified from frozen kidney tissue with the use of RNeasy Mini Kit (Qiagen Valencia, CA). Total RNA integrity was checked using an Agilent 2200 TapeStation (Agilent

Technologies, Inc., Santa Clara, CA) and quantified using a Trinean DropSense96 spectrophotometer (Caliper Life Sciences, Hopkinton, MA). RNA-seq libraries were prepared from total RNA using the TruSeq RNA Sample Prep Kit (Illumina, Inc., San Diego, CA, USA) and a SciClone NGSx Workstation (PerkinElmer, Waltham, MA, USA). Library size distributions were validated using an Agilent 2200 TapeStation (Agilent Technologies, Santa Clara, CA, USA). Additional library QC, blending of pooled indexed libraries, and cluster optimization were performed using Life Technologies' Invitrogen Qubit[®] 2.0 Fluorometer (Life Technologies-Invitrogen, Carlsbad, CA, USA).

RNA-seq libraries were pooled (6-plex) and clustered onto a flow cell lane. Sequencing was performed using an Illumina HiSeq 2500 in rapid mode employing a paired-end, 50 base read length (PE50) sequencing strategy. Image analysis and base calling were performed using Illumina's Real Time Analysis v1.18 software, followed by 'demultiplexing' of indexed reads and generation of FASTQ files, using Illumina's bcl2fastq Conversion Software v1.8.4 (http://support.illumina.com/downloads/bcl2fastq_conversion_software_184.html).

For RNA-seq data Analysis, reads of low quality were filtered prior to alignment to the reference genome (UCSC mm10 assembly) using TopHat v2.1.0[42]. Counts were generated from TopHat alignments for each gene using the Python package HTSeq v0.6.1[43]. Genes with low counts in greater than 2 samples were removed, prior to identification of differentially expressed genes using the Bioconductor package edgeR v3.12.0[44]. A false discovery rate (FDR) method was employed to correct for multiple testing[45]. Differential expression was defined as $\log_2(\text{ratio}) \geq 1$ (± 2 -fold) with the FDR set to 5%.

Transmission electron microscopy

Kidneys were harvested from 8 week-old *Fnip1*^{-/-} and *Fnip1*^{+/-} (wildtype) mice were chopped into ~ 1 mm³ pieces and preserved in Karnovsky's Gluteraldehyde fixative. Samples were dehydrated, sectioned into 70-100nm sections at the Vision Core Lab of the University of Washington (Seattle, WA). Tissue slices were epoxy embedded and visualized with the use of a JEOL 1230 transmission electron microscope (JEOL Ltd., Tokyo, JAPAN). 10 images were taken from low and high power fields per mouse. Percent mitochondrial area was calculated using ImageJ (National Institutes of Health) (17). The ratio of mitochondrial area/total area was determined for n = 4 mice per genotype (3 high quality low power fields (images) per mouse).

Flow cytometry. Mice were perfused with saline by gravity force following CO₂ euthanasia. Kidney tissues were harvested, diced with scissors into small pieces (~1mm diameter), and incubated with collagenase solution at 37 degrees for 30 minutes. Tissues were further dissociated using a syringe plunger and passed through 70µm cell strainer. Collected cells were lysed with ACK lysis buffer (to remove all red blood cell contamination), and stained with fluorescent-conjugated antibodies specific against CD3, B220, Gr1 [18]. Flow cytometric data were acquired on a FACSCanto II or LSRII flow cytometer (BD Biosciences), and data were analyzed using FlowJo software.

Statistics

Data were analyzed with the Student's two-tailed *t*-test. Kaplan-Meier curve statistics were performed with Log-rank Mantel-Cox test. Seahorse data were analyzed by paired *t*-test of the mean values for each time-point. For real-time quantitative PCR, differences were calculated using the comparative C_T method[36]. *p* < 0.05 were considered significant.

Results

Disruption of *Fnip1* results in increased kidney weight and renal cyst formation

Because inactivating mutations in the *BHD* gene encoding Folliculin result in renal cancer, we sought to determine if loss of *Fnip1* alters kidney development and/or function in *Fnip1*-null mice, which were previously generated using ENU chemical mutagenesis [18]. We first assessed kidney size by measuring kidney-to-brain weight ratios following disruption of *Fnip1*. We found that kidney-to-brain weight ratios were significantly greater in *Fnip1*^{-/-} mice (Fig 1A) compared to wildtype (WT) mice, indicating that loss of *Fnip1* results in increased kidney weight. Analyses of hematoxylin and eosin (H&E) stained histologic sections of kidney revealed that there were increased numbers of cysts (≥ 5X normal tubule diameter) and microcysts (<5x normal tubule diameter) in the renal cortex of *Fnip1*^{-/-} mice compared to WT mice (Fig 1B and 1C). The cysts and microcysts (hereafter collectively called cysts) were lined by renal tubular epithelium, which tended to form blebs into the cyst lumen. Loss of *Fnip1* did not change urine specific gravity relative to WT mice, suggesting that renal function was not perturbed following disruption of *Fnip1* (data not shown). These results collectively suggest that loss of *Fnip1* alters renal morphology, leading to the formation of cysts in the renal cortex.

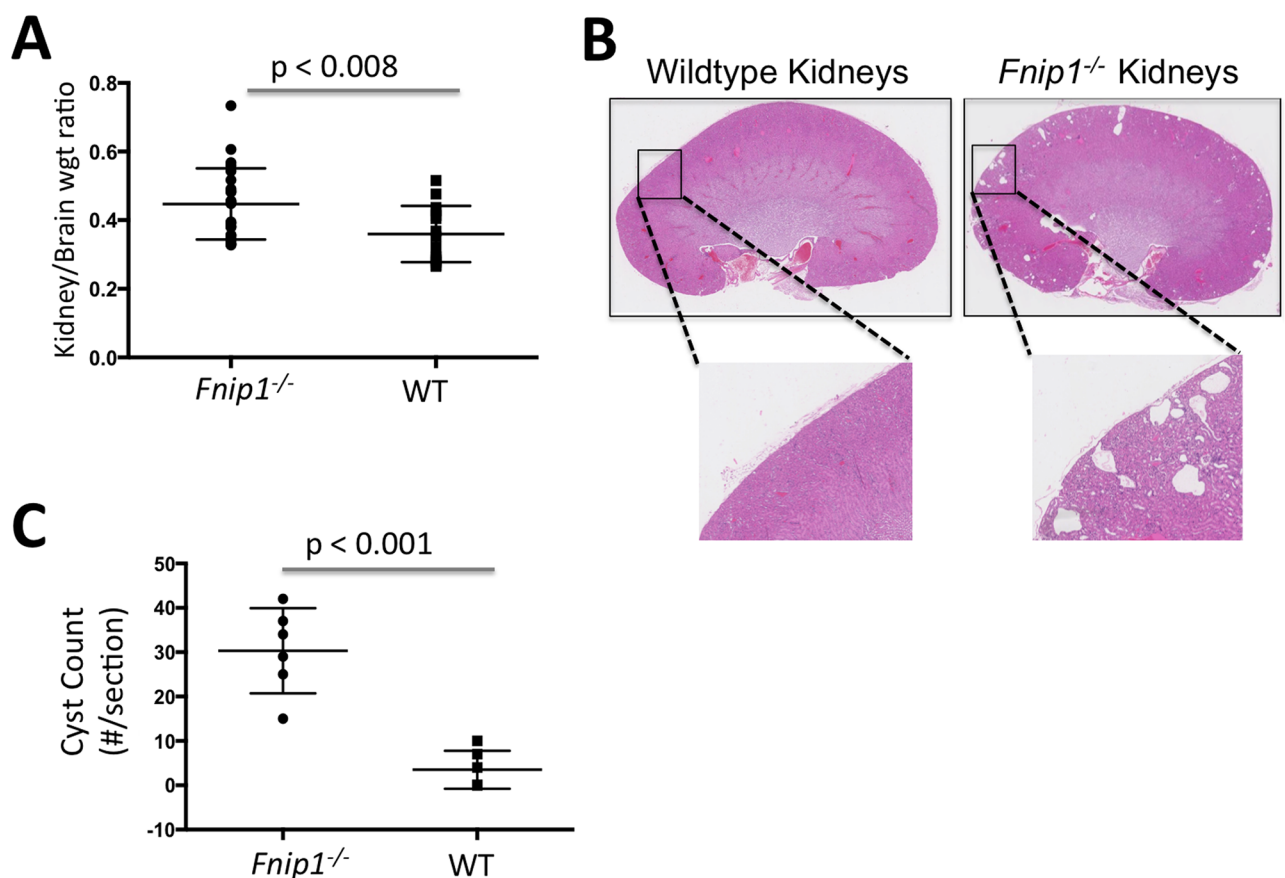


Fig 1. Loss of *Fnip1* results in increased kidney size and cyst formation. (A) Increased kidney-to-brain weight ratio in *Fnip1*^{-/-} versus wildtype mice. n = 15 mice per genotype. Shown are means +/- SEM. (B) Representative hematoxylin and eosin stained histology sections of *Fnip1*^{-/-} and wildtype kidneys. *Fnip1*^{-/-} mice develop cysts and microcysts in the renal cortex. (C) Graph showing cyst counts, as determined by a blinded counter, of 12–18 week-old *Fnip1*^{-/-} and WT mice (n = 6 per group). *p-values are shown.

<https://doi.org/10.1371/journal.pone.0197973.g001>

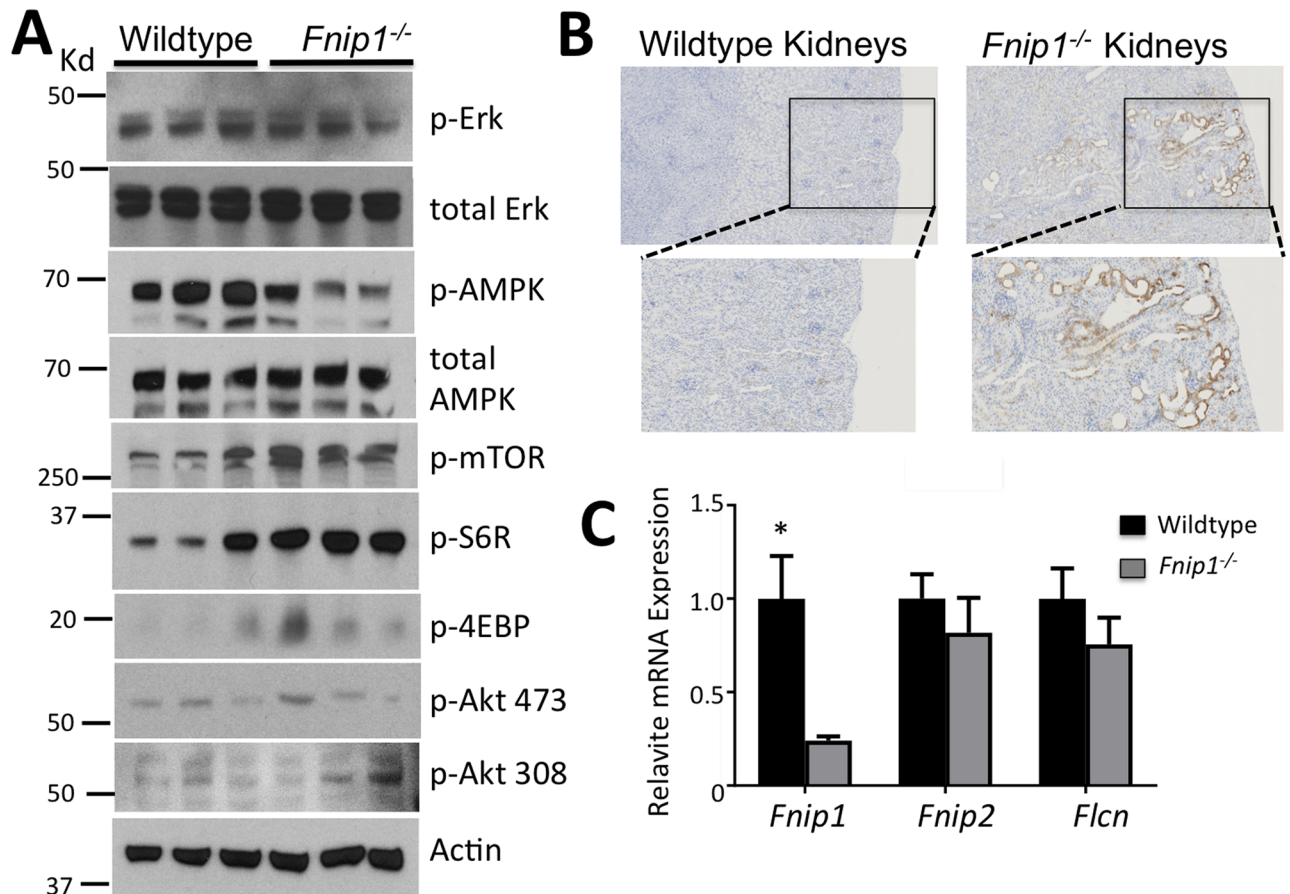


Fig 2. Increased mTOR and decreased AMPK activation in *Fnip1* null kidney tissue and renal tubular epithelial cells. (A) Representative immunoblots showing decreased AMPK activation (pAMPKThr172) and increased mTORC1 activation (p-S6R, p-4EBP1) in total renal tissue from *Fnip1*^{-/-} and WT mice. Statistical quantitation is shown in S1 Fig, n = 3 mice per genotype (each lane). (B) Representative immunohistochemistry images showing increased p-S6R activation around cystic tubules in *Fnip1*^{-/-} mice. Representative of 3 mice per genotype. (C) Real-time quantitative PCR showing no significant changes in expression of *Flcn* (*Bhd*) and *Fnip2* mRNA in *Fnip1*^{-/-} renal tissue versus WT (n = 3/genotype, * = p = 0.03). Mice used were between 12–18 weeks of age.

<https://doi.org/10.1371/journal.pone.0197973.g002>

Fnip1 loss results in decreased AMPK activation and increased mTORC1 activity

Disruption of the *Bhd* gene in mice results in polycystic kidney disease (PKD) characterized by altered mTORC1 activation. To determine why loss of *Fnip1* could result in increased renal weight and cyst formation, we measured activation of AMPK and the mTOR pathways by immunoblotting and immunohistochemistry (IHC). Immunoblotting of whole kidney lysate from *Fnip1*^{-/-} and WT mice revealed decreased phosphorylation of AMPK at threonine 172 indicative of decreased AMPK activation, increased phosphorylation of mTOR, and increased phosphorylation of S6 ribosomal protein (S6R), a downstream target of mTORC1 activation (Fig 2A and S1 Fig). Phosphorylation of Erk1/2, Akt^{Thr308}, and Akt^{Ser473} were not significantly different in *Fnip1*^{-/-} versus WT cells, suggesting no significant effect of *Fnip1* loss on Erk, PI3K, or mTORC2 signaling. Using IHC, we found local increases in p-S6R in the renal tubular epithelial (RTE) cells lining the cysts in the *Fnip1*^{-/-} kidneys (Fig 2B). mRNA expression of *Fnip2* and *Bhd* (*Flcn*) were unchanged (Fig 2C) in *Fnip1* null kidneys, indicating that the phenotypes

are not due to secondary alterations in their expression. These results indicate that loss of *Fnip1* results in decreased AMPK activation and increased mTORC1 activation in RTE cells.

***Fnip1* deficient renal epithelial cells exhibit increased oxidative phosphorylation**

Both PKD and renal cancer exhibit metabolic changes characterized by increased glycolysis and/or oxidative phosphorylation. We next assessed whether loss of *Fnip1* and subsequent mTORC1 activation altered the metabolic characteristics of *Fnip1* null renal tubular epithelial cells. RTE cells were isolated from *Fnip1*^{-/-} and WT mice, and basal metabolic characteristics were measured using the Seahorse XF analyzer, which measures oxygen consumption rate (OCR; a measure of oxidative phosphorylation) and extracellular acidification rate (ECAR; a measure of glycolysis). *Fnip1*^{-/-} RTE cells exhibited increased maximal OCR (Fig 3B) relative to WT renal tubular epithelial cells following FCCP (carboxy cyanide-4 trifluoromethoxy phenylhydrazine) stimulation (a mitochondrial membrane uncoupler), indicating that loss of *Fnip1* results in increased maximal respiration. Although not significantly different ($p = 0.06$), there was a trend towards increased glycolysis following *Fnip1* loss.

In order to better define this observed metabolic shift, we took an unbiased broad-based metabolomic approach using liquid chromatography tandem mass spectrometry (LC-MS/MS) to measure alterations in levels of metabolites associated with major metabolic pathways. We found that *Fnip1*^{-/-} kidneys contained increased levels of metabolites derived from the amino acid leucine (D-Leucic acid, 2-hydroxyisovaleric acid, and OH-phenylpyruvate), a major inducer of mTORC1 activation, relative to WT kidneys (Fig 3C and 3D and S1 Table). *Fnip1*^{-/-} kidneys also exhibited increased levels of glycolysis and TCA cycle metabolites including dihydroxyacetone phosphate (DHAP) and oxaloacetate respectively. Increases were also seen in the purine metabolites 1-methyladenosine and allantoin (Fig 3C and 3D and S1 Table), consistent with increased purine biosynthesis in *Fnip1*^{-/-} kidneys. Interestingly, 1-methyladenosine is elevated in the urine of patients with malignant cancers [46, 47], and promotes translation of methylated mRNAs leading to increased protein production [48]. These results support increased metabolic activity following disruption of *Fnip1* (Fig 3), and are also consistent with increased mitochondrial biogenesis, oxidative phosphorylation, glycolysis, and purine biosynthesis (see [49] for review).

Global gene expression analyses reveal alterations in ion transporters, cell adhesion molecules, and immune cell infiltration

To assess global mRNA changes associated with disruption of *Fnip1* in renal tissue, we performed RNAseq on cortical kidney tissue from *Fnip1*^{-/-} and *Fnip1*^{+/-} mice, followed by quantitative PCR to assess changes in gene expression of selected genes of interest. We found that mRNA expression of 651 genes were significantly different in *Fnip1*^{-/-} kidney tissue versus *Fnip1*^{+/-} tissue. Of the 651 genes, expression of 445 genes were upregulated and 206 genes were downregulated following disruption of *Fnip1*. Kyoto Encyclopedia of Genes and Genome (KEGG) analyses indicated that of the downregulated genes, there was significant enrichment for genes associated with sodium independent ion transport, organic ion transport, anion transmembrane transport, and lipid metabolism (Fig 4A and 4B and S2 Table). In contrast, of the upregulated genes, there was significant enrichment in expression of genes associated with cell adhesion and immune response (Fig 4C and S2 Table). While it is formally possible that some of these mRNA changes may reflect differences in the representation of specific cell types in cortical tissue from *Fnip1*^{+/-} versus *Fnip1*^{-/-}, the vast majority of RNA is derived from

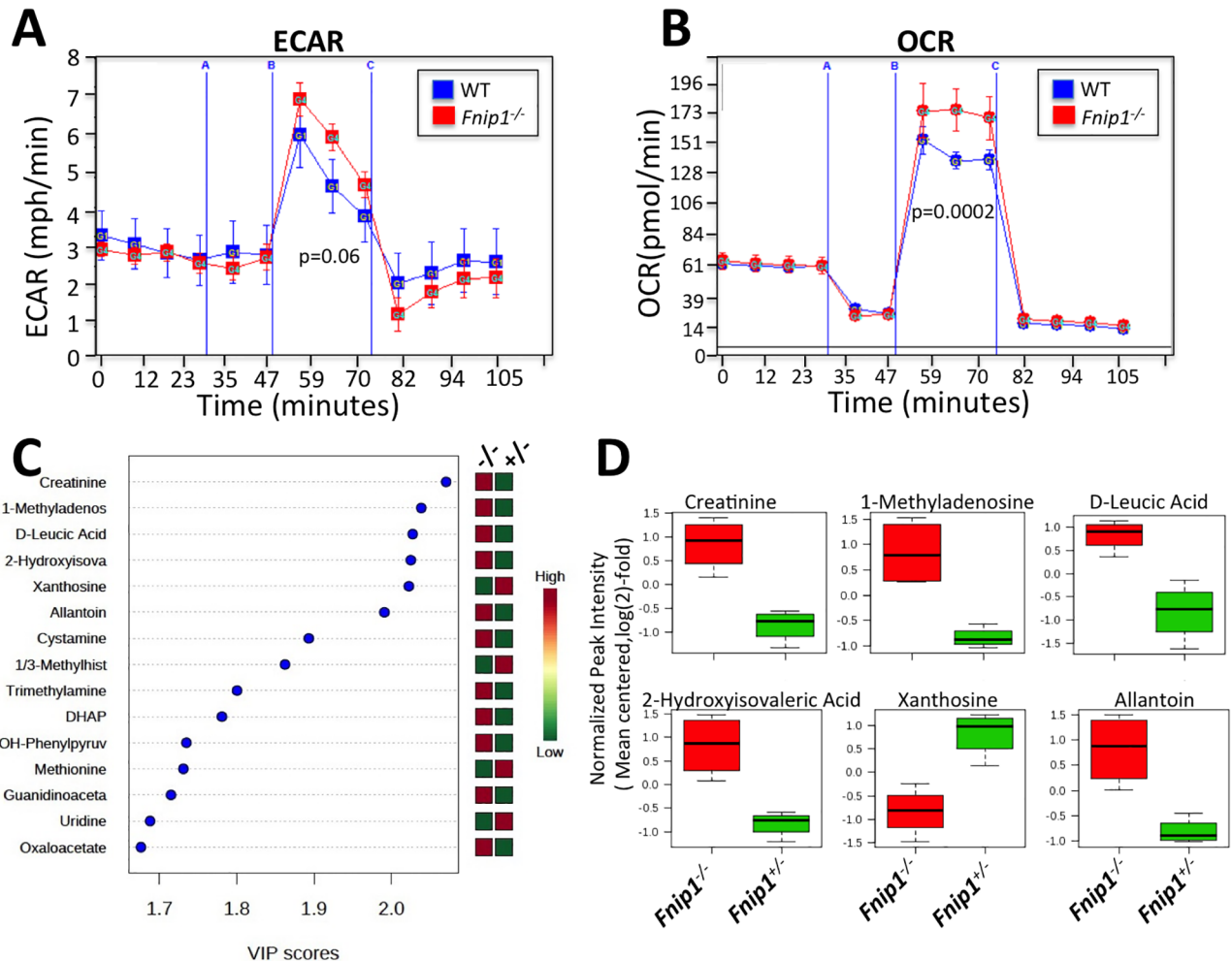


Fig 3. *Fnip1*^{-/-} kidney tubular epithelial cells exhibit increased metabolism. (A) Seahorse analyses showing increased maximal extracellular acidification rate (ECAR), a measure of glycolysis, and (B) increased maximal oxidative phosphorylation (OCR) of cultured purified *Fnip1*^{-/-} (n = 3 mice) versus WT (n = 3 mice) renal tubular epithelial cells. Cells were stimulated with oligomycin (2.5 μM) at 30 minutes, FCCP (0.5 μM) at 50 minutes, and rotenone (2 μM) and antimycin A (2 μM) at 75 minutes. p-values are shown. (C and D) Total kidneys from *Fnip1*^{-/-} (n = 4) and WT (n = 3) mice (20–32 weeks old) were analyzed by liquid chromatography tandem mass spectrometry (LC-MS/MS) to determine metabolite levels. Data were analyzed using MetaboAnalyst 3.0. Variable importance in projection (VIP) scores of metabolite changes in *Fnip1*^{-/-} versus wildtype renal tissue showing changes in nitrogenous waste products, amino acid metabolites, glycolysis, and TCA cycle metabolites. Metabolites that were significantly different and either increased (red) or decreased (green) are shown. (D) Whisker plots showing selected metabolites either significantly increased or decreased in *Fnip1*^{-/-} (red) versus *Fnip1*^{+/-} (green) kidney tissue. p-values are listed in S1 Table.

<https://doi.org/10.1371/journal.pone.0197973.g003>

similar renal cortical cell types (tubular epithelial cells, glomerulus parietal cells, podocytes, etc) which likely reflect the majority of transcriptional differences.

Quantitative PCR analyses confirmed that expression of many *Slc* family of transporter genes were downregulated following disruption of *Fnip1* (S2 Table and Fig 5A). For example, expression of *Slc1a4* and *Slc17a3*, which are involved with glutamate transport, were both significantly decreased in *Fnip1*^{-/-} versus *Fnip1*^{+/-} tissue. Similarly, expression of *Slc13a5*, and *Slc24a3*, genes involved with Na⁺ transport, were also decreased in *Fnip1*^{-/-} versus *Fnip1*^{+/-} tissue. Genes important for the transport of organic molecules in the proximal renal tubule were also decreased including *Slc22a2*, which resorbs organic cations; *Slc22a6* and *Slc22a7*, which are involved with the transport of anions; and *Slc22a12*, which transports urate for excretion and is important for proper kidney function. Of the *Slc* genes with increased expression,

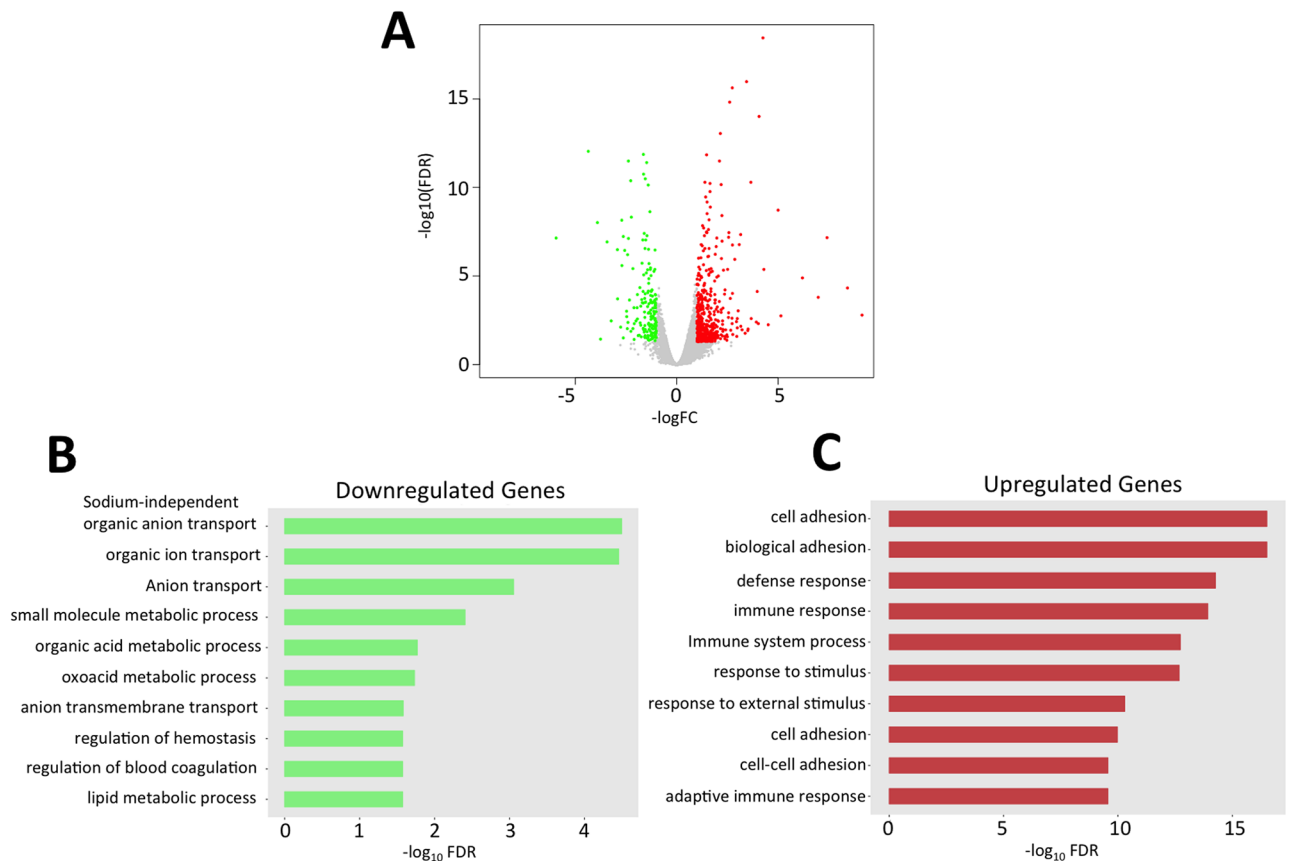


Fig 4. Differences in gene expression between *Fnip1*^{-/-} versus wildtype kidney tissue. RNAseq was performed on kidney cortical tissue from *Fnip1*^{-/-} (n = 3) and wildtype (n = 3) mice (11–18 weeks of age) using Illumina HiSeq 2500. (A) Volcano plot generated using EdgeR program showing genes significantly increased (red) and decreased (green) in *Fnip1*^{-/-} kidney versus WT kidney tissue. Gene ontology analyses derived from Bioconductor Open Source Software for Bioinformatics showing: (B) significantly downregulated genes grouped by expression levels and gene function in *Fnip1*^{-/-} compared to WT renal tissue, and (C) significantly upregulated expression of genes grouped by expression levels and gene function in *Fnip1*^{-/-} compared to WT renal tissue. The majority of significantly decreased genes were involved in ion transport and metabolism, whereas the majority of significantly increased genes were involved in cell adhesion and immune responses.

<https://doi.org/10.1371/journal.pone.0197973.g004>

Slc15a3 is a proton/oligopeptide cotransporter, and *Slc22a3* is an organic cation transporter that is expressed in several tissues including liver, intestine, nervous, and kidney. These results collectively suggest that loss of *Fnip1* in renal tissue results in significant alterations in the expression of an array of integral membrane ion transporters.

Our Seahorse and metabolomics analyses suggested that mitochondrial metabolism is increased in *Fnip1* null tissue. Consistent with this notion, RNAseq and quantitative PCR data showed changes in multiple genes involved in Acyl-CoA pathway and fatty acid metabolism (Figs 5B and S2). For example, expression of *Acox3*, *Acsm 3*, and *CD36*, which are all involved with fatty acid synthesis, were decreased in *Fnip1*^{-/-} mice, whereas expression of genes associated with fatty acid binding and shuttling were increased, including *Fabp1*, *Fabp4*, *Perilipin1*, and *Perilipin 4* (S2 Table and Fig 5). Expression of *Acsc1* (acetyl-CoA synthetase), which is important in the TCA cycle was increased, while expression of *Acot12*, which hydrolyzes Acetyl CoA, was decreased. These increases in metabolites and the changes seen in expression of Acyl-CoA genes are consistent with increased mitochondrial metabolism. To determine whether mitochondrial density or morphology was altered following disruption of *Fnip1*, we performed electron microscopy on renal tissue from *Fnip1*^{-/-} and WT mice. Although no

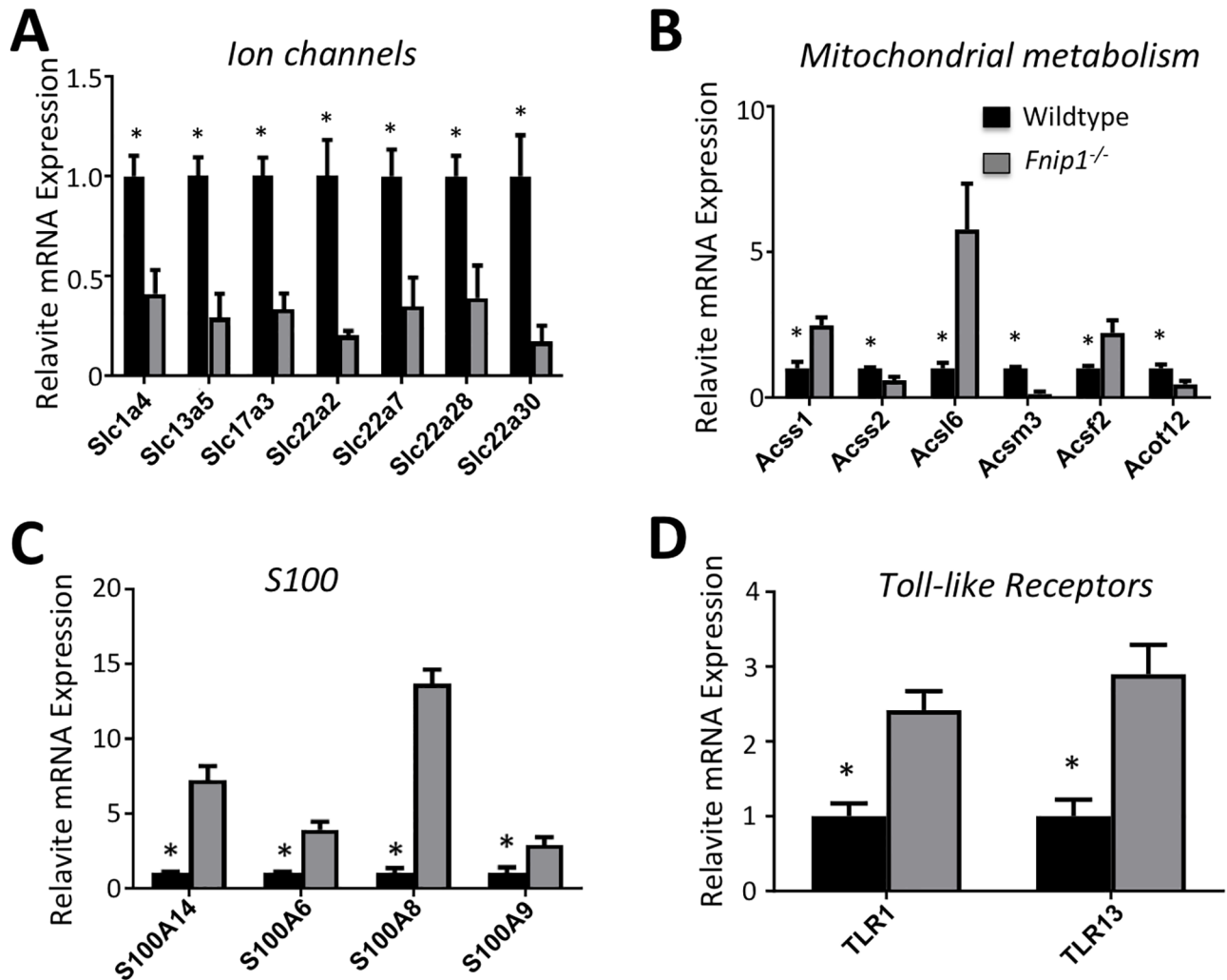


Fig 5. Real-time Quantitative PCR analyses on kidney tissue from *Fnip1*^{-/-} versus wildtype mice. RNA was purified from *Fnip1*^{-/-} (n = 3) compared to WT (n = 3) kidney cortical tissue (mice were 11–18 weeks of age). Quantitative PCR was performed on cDNA derived from these tissues. Bar graphs show fold- differences in gene expression in *Fnip1*^{-/-} compared to WT mice (where WT is set to 1). (A) Genes encoding many of the solute carrier (Slc) family of transporter proteins are decreased in *Fnip1*^{-/-} compared to WT kidney tissue. (B) Altered expression of genes encoding acyl-CoA regulatory molecules and fatty acids regulatory molecules. (C) Expression of S100A genes including A14, 6, 8, and 9 are increased in *Fnip1*^{-/-} compared to WT kidney tissue. (D) Increased expression of TLR1 and 13 genes in *Fnip1*^{-/-} compared to WT kidney tissue. (n = 3 of each genotype, * = p<0.01).

<https://doi.org/10.1371/journal.pone.0197973.g005>

statistically significant changes were noted, there was a trend towards increased mitochondrial area in *Fnip1*^{-/-} RTE cells relative to WT cells (S2 Fig).

To define how loss of *Fnip1* alters mRNA expression, we utilized the Ingenuity Upstream Regulator Analyses program to help illuminate the cascade of transcriptional regulators that are differentially regulated in the RNAseq data derived from *Fnip1*^{-/-} vs wildtype kidney tissue [50]. Interestingly, we found that loss of *Fnip1* resulted in the most significant enrichment for Myc-regulated genes, followed by HDAC1, HDAC2, FoxA1, and HoxA10, which were predicted to be activated based on the direction of the gene expression change following disruption of *Fnip1* (S3 Table). Other transcriptional regulators with significant enrichment included Spi1, Ets1, Creb, HTT, PGC1alpha, and TP63. Although Ingenuity was unable to predict activation versus repression for PGC1alpha or Myc in our RNAseq study (likely because the program does not take into account the presence or absence of co-activators, co-repressors, or

dominating repressive complexes), increased Myc and PGC1alpha expression have been associated with PKD and renal cancer [17, 51, 52].

Recent studies suggest that increased kidney inflammation is associated with PKD in humans [53, 54]. RNAseq and quantitative PCR revealed that genes involved in immunity and inflammation were increased in *Fnip1*^{-/-} renal tissue relative to WT renal tissue, including the S100, Toll-like receptors (TLR), NOD-like receptors, FC-receptors, MHC, and genes encoding complement (Fig 5C and 5D and S2 Table). Specifically, *Fnip1*^{-/-} renal tissue was characterized by increased expression of complement components including component 3 (*C3* and *C3ar1*), which are important in both the classical and alternate pathways of complement signaling, and *C1qa*, *b*, and *c*, which are all part of the *C1q* complex that is important in the classical pathway (S2 Table). Similarly, increases were seen in the expression of the *S100A14*, *S100A6*, *S100A8*, and *S100A9* pro-inflammatory genes (Fig 5C and S2 Table). *S100A14* affects the p53 pathway and modulates expression of matrix metalloproteases MMP1 and MMP9. *S100A6* functions in cell proliferation, cytoskeletal dynamics, and tumorigenesis, thus promoting cell division and tumor growth. *S100A8* is highly expressed in the cytosol of some immune cells including neutrophils, macrophages, and dendritic cells, and is induced by toll-like receptor (TLR) agonists, and *S100A9* inhibits myeloid differentiation thereby contributing to tumor growth. We also found that expression of *Tlr1*, *Tlr7*, and *Tlr13* were also increased in *Fnip1*^{-/-} versus WT kidney tissue (Fig 5D and S2 Table). Toll-like receptors are important for activation of the innate immune system by recognizing pathogen-associated molecular patterns in microbes.

To further determine whether disruption of *Fnip1* was associated with increased inflammation in *Fnip1* null renal tissue, we purified immune cells from *Fnip1*^{-/-} and *Fnip1*^{+/-} kidney tissue and defined the representation of specific immunocytes by flow cytometry. Compared to *Fnip1*^{+/-} renal tissue, *Fnip1*^{-/-} renal tissues exhibited a significant increase in the representation of CD11c⁺ and GR1⁺ myeloid cells (Fig 6A), whereas the percentages of total CD3⁺ T cells were not significantly different. B220⁺ B cells were decreased following disruption of *Fnip1*, due to a block in B cell development [18]. CD11c is an integrin expressed on monocytes, macrophages, and neutrophils, and GR1 protein is predominantly expressed on bone marrow and peripheral blood neutrophils. Interestingly, using IHC we found focal increases in F4/80 staining localized around the cysts in sections of kidney from *Fnip1*^{-/-} relative to WT mice (Fig 6B). The F4/80 antigen is a glycoprotein that is expressed by murine macrophages. In contrast to our data on the representation of T cells in total renal tissue, we found focal increases in CD3epsilon positive T cells around renal cysts as well (Fig 6C). These results suggest that disruption of *Fnip1* results in increased representation of inflammatory cells infiltrating *Fnip1* deficient kidney tissue, which appears to be localized around renal cysts.

Fnip1 and Tsc1 synergize to inhibit mTORC1 activation and polycystic kidney disease

Kidney tissues from human patients with BHDS, and murine kidney tissue from mice with gene-targeted mutations in *Bhd*, are generally characterized by increased mTORC1 activation. However, recent studies whereby *BHD*, *FNIP1*, or *FNIP2* were knocked down in cell lines suggested that the Folliculin/Fnip1/Fnip2 complex may be required to activate mTORC1 [24, 25]. To further assess how disruption of *Fnip1* modifies mTORC1 signaling and PKD in vivo, we generated a murine model of PKD, whereby the mTORC1 inhibitor *Tsc1* gene was disrupted using *Mb1Cre*, which is predominantly expressed in hematopoietic cells and to a lesser extent in kidney [32]. We then bred *Fnip1*^{-/-} mice to *Tsc1*^{fl/fl}*Mb1Cre* mice to define the consequences of *Fnip1* loss on hyperactive mTOR signaling and the development of PKD driven by *Tsc1* loss. *Tsc1*^{fl/fl}*Mb1Cre* mice alone developed significant PKD by 10 weeks of age (Fig 7A and 7B)

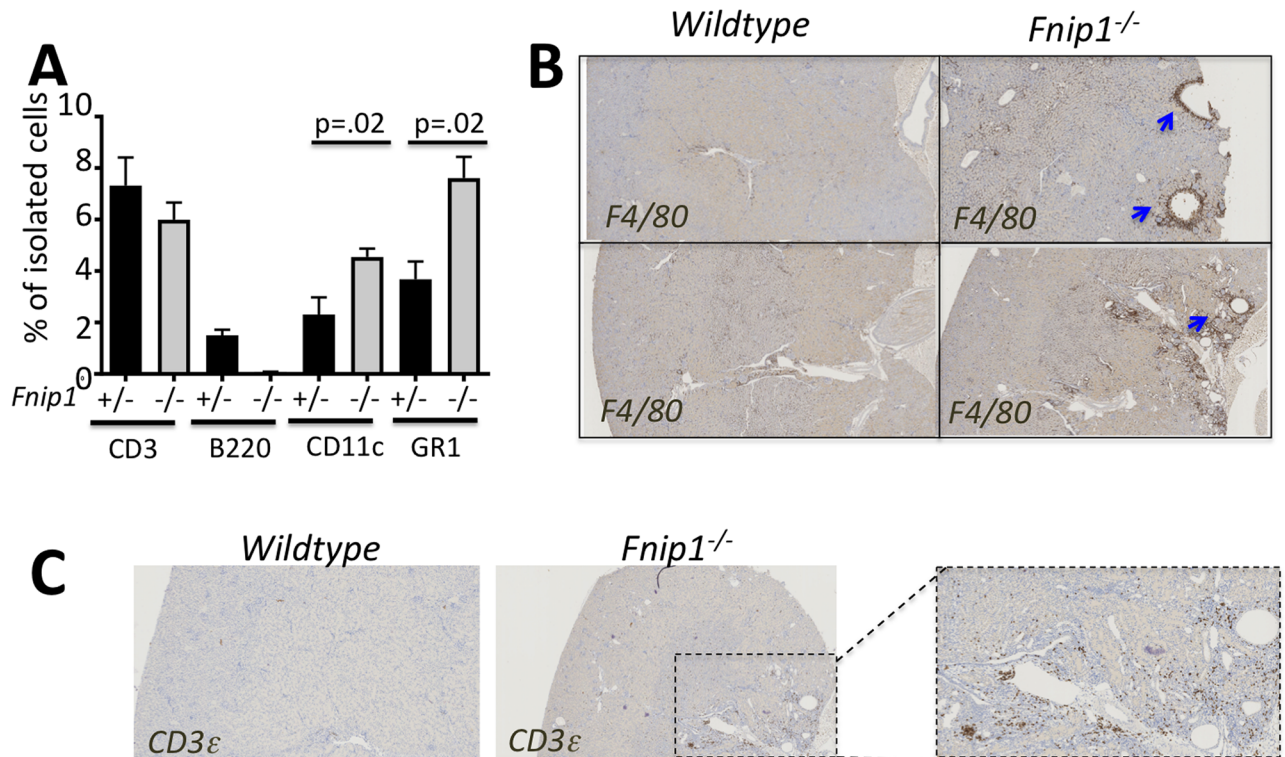


Fig 6. Increased immune cell infiltration in *Fnip1*^{-/-} null kidney tissue. (A) Flow cytometric analyses of immune cells isolated from *Fnip1*^{-/-} and wildtype kidney tissue showing increases in the representation of CD11c and GR1 labeled cells and decreases in B220 labeled cells (n = 3 of each genotype, p-values are shown). (B) Representative immunohistochemistry images showing increased representation of F4/80⁺ myeloid cells and (C) increased representation of CD3⁺ cells localized around renal cysts of *Fnip1*^{-/-} mice (arrows). Micrographs are representative of 3 mice per group (~12 weeks of age).

<https://doi.org/10.1371/journal.pone.0197973.g006>

characterized by a ~ 2-fold increase in kidney/brain weight ratio and increased cystic structures at 10 weeks of age, which progressed to a ~5-fold increase in kidney/brain weight by 20 weeks of age (Fig 7C). *Tsc1*^{fl/fl}*Mb1Cre* mice also exhibited decreased survival, which could be completely rescued by provision of a rapamycin diet (Fig 7D). Analyses of renal tissue from 12 week-old *Tsc1*^{fl/fl}*Mb1Cre* and age-matched WT mice revealed significantly increased Erk-phosphorylation (Figs 7E and S4). Phosphorylation of S6R and 4E-BP1, downstream targets of mTORC1 signaling, were also significantly increased in *Tsc1*^{fl/fl}*Mb1Cre* mice relative to age-matched wildtype mice.

To define how loss of *Fnip1* modulates activated mTOR signaling in *Tsc1* null mice, we measured kidney-to-brain weight ratios in *Fnip1*^{-/-}*Tsc1*^{fl/fl}*Mb1Cre* double-null mice (*Fnip1**Tsc1* double-null) mice compared to *Tsc1*^{fl/fl}*Mb1-Cre*⁺ mice alone. *Fnip1**Tsc1* double-null mice developed large cystic kidneys (kidney/brain ratio mean 1.79) by 4 weeks of age (Fig 8A and 8B) whereas *Tsc1* null mice had normal appearing kidneys at 4 weeks (Figs 8A and 7C), and did not develop cystic kidneys of comparable kidney/brain weight ratio as *Tsc1**Fnip1* double null mice until ~10 weeks of age. While the *Tsc1* null mice survived an average of 24 weeks until euthanasia (Fig 7D), *Tsc1**Fnip1* double null mice only survived to 3–5 weeks of age before euthanasia was required (Fig 8C). Immunoblot analysis revealed increased phosphorylated Erk and decreased phosphorylated AMPK^{Thr172} in *Tsc1**Fnip1* double null kidneys relative to *Tsc1*^{-/-} and WT kidneys. mTORC1 activation, as measured by phosphorylation of mTOR, ribosomal

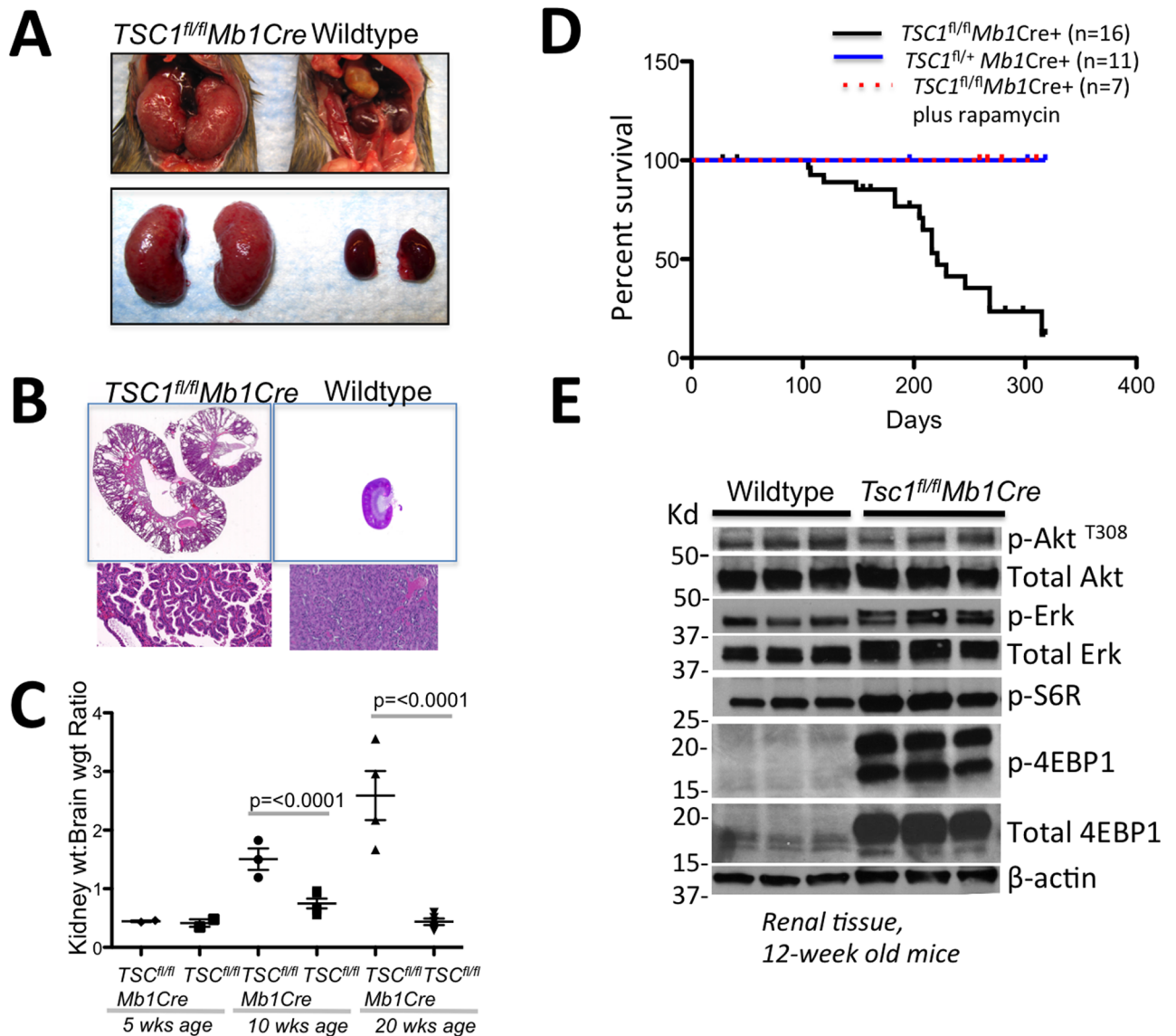


Fig 7. Conditional disruption of *Tsc1* results in polycystic kidney disease. *Tsc1^{fl/fl}* mice were bred to *Mb1Cre⁺* mice. (A) Representative gross pictures of *Tsc1^{fl/fl} Mb1Cre⁺* and WT kidneys showing that loss of *Tsc1* results in kidney enlargement in 20-week old mice. (B) Representative histology images of *Tsc1^{fl/fl} Mb1Cre⁺* kidneys showing development of polycystic kidney disease at 20 weeks of age. (C) Kidney-to-brain ratio graph showing ratios at 5, 10, and 20 week old *Tsc1^{fl/fl} Mb1Cre⁺* and WT mice showing a gradual increase in kidney-to-brain weight ratio in *Tsc1^{fl/fl} Mb1Cre⁺* kidneys. (n = 3 each genotype, p-values are shown) (D) Survival graph of *Tsc1^{fl/fl} Mb1Cre⁺* (solid black line), *Tsc1^{fl/+} Mb1Cre⁺* (solid blue line), and rapamycin treated *Tsc1^{fl/fl} Mb1Cre⁺* (dotted red line) showing that polycystic kidney disease is fatal, but that disease induction can be blocked by inhibiting mTOR with Rapamycin. Rapamycin diet was started at weaning and continued until euthanasia. (E) Immunoblots of proteins isolated from whole kidney lysates from 12-week old mice showing increased p-S6R and p-4EBP1 indicative of increased mTORC1 activation, and increased p-Erk in *Tsc1^{fl/fl} Mb1Cre⁺* relative to WT kidney tissue.

<https://doi.org/10.1371/journal.pone.0197973.g007>

S6 protein (S6R), and 4E-BP1 were increased in *Tsc1^{-/-} Fnip1^{-/-}* double null mice relative to *Tsc1^{-/-}* and WT mice (Figs 8D and S4). Interestingly, phosphorylated EIF4E-binding protein 1 (p-4E-BP1) levels were approximately 10-fold higher than either *Tsc1^{-/-}* or WT kidneys. These results indicate that there is strong synergism between loss of *Fnip1* and loss of *Tsc1*, and suggest that loss of these pathways utilize divergent mechanisms to activate mTORC1 in vivo in the absence of transformation.

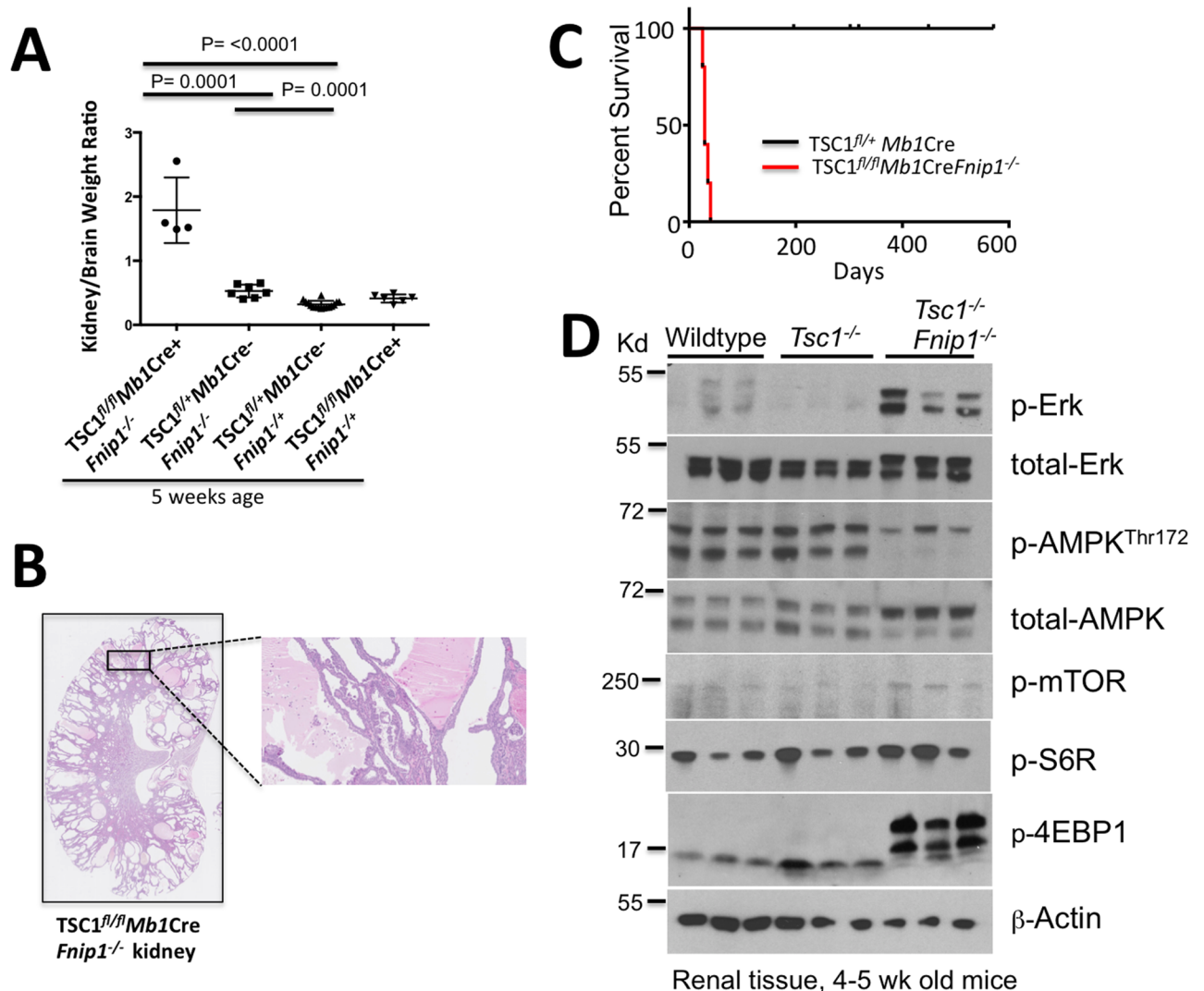


Fig 8. Loss of Fnip1 synergizes with loss of TSC1 resulting in accelerated PKD and mTOR activation. (A) Kidney-to-brain ratio graph comparing double null ($Tsc1^{fl/fl}Mb1Cre^+Fnip1^{-/-}$), $Fnip1^{-/-}$ ($Fnip1^{-/-}Tsc1^{fl/fl}Mb1Cre^-$), $Tsc1$ null ($Fnip1^{+/+}Tsc1^{-/-}Mb1Cre^+$), and heterozygous ($Fnip1^{-/+}Tsc1^{fl/fl}Mb1Cre^-$) mice at 5 weeks of age, showing an increase in kidney size of double null mice at an early age. (B) Representative histology image of $Tsc1^{fl/fl}Mb1Cre^+Fnip1^{-/-}$ double null mice showing the development of severe polycystic kidney disease at 5 weeks of age. (C) Kaplan Meier survival graph of $Tsc1^{fl/fl}Mb1Cre^+Fnip1^{-/-}$ double null and $Tsc1^{fl/fl}Mb1Cre^+Fnip1^{+/+}$ mice. Double-null mice develop PKD very early in life, indicating that loss of $Fnip1$ in $Tsc1$ null mice greatly accelerates the onset of PKD relative to $Tsc1$ loss alone. (D) Immunoblots of proteins isolated from whole kidney lysates derived from 5 week-old wildtype, $Tsc1^{-/-}$, and $Tsc1^{-/-}Fnip1^{-/-}$ blots showing increased p-Erk, p-S6R, and p-4E-BP in $Tsc1^{-/-}Fnip1^{-/-}$ kidney tissue compared to $Tsc1^{-/-}$ and WT mice indicating hyperactivation of the mTORC1 and Erk pathways. p-AMPK is decreased in double null mice relative to $Tsc1^{-/-}$ and WT mice, suggesting decreased AMPK activation. (n = 3 each genotype, p-values are shown).

<https://doi.org/10.1371/journal.pone.0197973.g008>

Discussion

Although disruption of Folliculin is known to predispose to renal cancer in humans, and PKD and renal cancer in mice, a specific role for Fnip1 has not been previously demonstrated. In this study, we found that disruption of *Fnip1* alone results in renal cyst formation and was surprisingly sufficient to initiate many of the molecular and cellular changes implicated in the development of PKD in humans, including decreased expression of organic ion transporters; increased oxidative metabolism; increased cellular growth; increased expression of cell adhesion molecules; and increased immune cell infiltration in areas directly surrounding cysts. We

also provide evidence that *Fnip1* normally synergizes with *TSC1* to limit mTORC1 activation in renal tissue, thus mitigating the development of PKD. These results provide support that *Fnip1* regulates a large functional molecular network in renal epithelial cells, which when disrupted, contributes to PKD and cancer.

Many of the cellular and molecular features of PKD have been characterized, although the molecular mechanisms of how these alterations result in PKD are still unclear. However, changes in signaling pathways that result in increased renal tubular epithelial cell proliferation, including activation of the mTOR and Ca^{2+} pathways, are primary features. For example, autosomal dominant polycystic kidney disease (ADPKD) in humans is characterized by the development of fluid filled kidney cysts, which eventually destroy normal kidney function and progress to renal failure. ADPKD is caused by mutations in either the *PKD1* or *PKD2* genes, which encode Polycystin 1 (PC1) and Polycystin 2 (PC2) respectively (see [55] for review). PC1 is found in the primary renal cilia where it localizes to the plasma membrane and forms adhesion complexes in polarized epithelial cells. PC1 is primarily important for cell-cell and cell-matrix interactions. PC2 is also a transmembrane protein that co-localizes with PC1 in the primary cilium. However, a large portion of PC2 is also localized in the intracellular compartment where it functions as a calcium permeable non-selective cation channel. The PC1-PC2 complex on the surface of cilia have been proposed to be activated by waves of fluid flow, which then transmits intracellular signals leading to mTORC1 activation[56] and calcium release from intracellular stores. Mutations in *PKD1* or *PKD2* have been hypothesized to alter intracellular signaling and cell matrix interactions, resulting in kidney epithelial cell reorganization into spherical rather than tubular structures, which then fill with fluid and expand the developing cysts (see [57] for review). One model for how tubular epithelial cells reorganize from tubular to spherical morphology posits that loss of cell polarity (through changes in cell adhesion) causes epithelial cells to stop dividing along the axis parallel to the tubule lumen, and divide excessively in a circular pattern[57] (S3 Fig).

Increased division of renal tubular epithelial cells is driven in part by increased activation of mTORC1 (see [55, 58] for review), a major driver of cellular growth. Previous studies have shown a link between PC1 and mTORC1, whereby the cytoplasmic tail of PC1 interacts with Tuberin, the protein product of the *TSC2* gene. It has been proposed that PC1 sequesters the mTORC1 complex together with Tuberin, which in turn inhibits mTOR activity [59, 60]. Mutations in PC1 release Tuberin from mTOR, allowing mTORC1 to translocate to the lysosome where it is activated [61]. Another proposed mechanism for mTORC1 activation in ADPKD is due to co-deletion of the *TSC2* gene along with *PKD1*, since both are located adjacent to each other on the human chromosome 16[58]. In various murine models of ADPKD, mTORC1 is significantly hyper-activated in kidney tissue, and inhibition of mTORC1 with rapamycin can significantly inhibit or reduce the severity of PKD[59, 62, 63]. mTORC1 has also been shown to negatively regulate the production of PC-1 and trafficking of the PC-1/2 complex to the cilia[60]. In this study, we found that loss of *Fnip1* was sufficient to increase mTORC1 activation primarily in renal epithelial cells lining renal cysts. Increased mTORC1 activation in this context was associated with increased expression of cell adhesion molecules, which are known to effect cell polarity during division[57]. These results collectively suggest that loss of *Fnip1* may contribute to PKD in part by increasing mTORC1 activation and upregulating expression of cell adhesion molecules, which together could alter cell polarity and promote cell division into spherical rather than tubular structures (S3 Fig).

Another major driver of increased epithelial cell division in ADPKD is the proto-oncogene *c-Myc*, whose expression is also increased in mouse models of PKD[55]. One study showed that transgenic expression of *c-Myc* is sufficient to cause cyst formation in primary murine kidneys[51]. Both *c-Myc* and mTOR are major drivers of the Warburg Effect, whereby cancer

cells switch their metabolic preferences from oxidative phosphorylation, which produces mostly ATP, to aerobic glycolysis, which generates precursors such as amino acids, nucleic acids, and lipids required to fuel cell division (see [64] [49] for review). Importantly, increased aerobic glycolysis has been also linked to ADPKD [56, 65, 66]. Increased glycolysis in PKD is also through loss of LKB1, which functions in part to activate AMPK[67] and inhibit mTOR[56]. Kidney specific deletion of *Lkb1* results in impaired AMPK activation, excessive mTORC1 activation, and the development of renal cysts[67]. Treatment of kidney specific *Lkb1*-null mice with non-metabolizable 2-deoxyglucose (2-DG) inhibits glycolysis and limits cyst formation. Metformin, a pharmacological activator of AMPK, inhibits both CFTR and mTOR pathways, and significantly arrests the growth of renal cysts *in vitro* and *in vivo*[68]. In this study, we found that loss of *Fnip1* resulted in decreased AMPK activation; increased mTORC1 activation; increased oxidative phosphorylation, and increased expression of genes regulated by the mTORC1 targets PGC1alpha and Myc in *Fnip1*^{-/-} versus WT kidney tissue. The PGCalpha transcriptional regulator is a major driver of mitochondrial biogenesis and oxidative phosphorylation, whereas c-Myc stimulates glycolysis. These results are consistent with *Fnip1* regulating epithelial cell proliferation and metabolism, in part through regulation of AMPK, PGCalpha, mTORC1, and c-Myc, which in turn stimulate mitochondrial biogenesis, OXPHOS, aerobic glycolysis, and cellular growth.

Other signaling pathways activated by the PC1/PC2 complex and are believed to modulate ADPKD, include activation of the Janus kinases (JAK) and Signal Transducers of Activated T cells (STAT/STAT3) transcription factors, which have been shown to both inhibit and stimulate renal epithelial cell division[69, 70]; activation of Ras/Raf/Erk signaling[71–73], which modifies proliferative and apoptotic stimuli; and activation of non-canonical Wnt signaling [74–76], which promotes cell polarity (for review see [57]). In this study, we found that disruption of *Fnip1* synergizes with *Tsc1* loss to increase Erk phosphorylation in *Fnip1*^{-/-}*Tsc1*^{-/-} kidney tissue versus *Fnip1*^{-/-} or *Tsc1*^{-/-} kidney tissue, suggesting that the Ras/Raf/Erk pathway is activated. In addition, we found both Stat1 and Stat3 target genes were significantly decreased in *Fnip1* null versus WT kidney tissue. mRNA expression of Frizzled B (*Fzlb*), the receptor for Wnt, was significantly decreased and Wnt inhibitor factor 1 (*Wif1*) was significantly increased in *Fnip1* null versus WT kidneys. These results suggest that decreased Stat1/3 (which would result in decreased p21 and increased cell cycle progression[70]), decreased Wnt signaling (which would result in decreased polarity), and increased Erk signaling (which would promote mTORC1 activation by inhibitory phosphorylation of TSC2[77]) may contribute to the development of PKD following disruption of *Fnip1*.

Following reorganization of epithelial cells into spherical cysts due in part to excessive cell proliferation, conversion from an ion absorptive to an ion secretory epithelium has been proposed to cause ion secretion into the cyst lumen, resulting in passive fluid accumulation[57, 78] (S3 Fig). In ADPKD, the ion secretory epithelium is defined by many changes in expression of ion channels including the cAMP activated cystic fibrosis transmembrane receptor (CFTR) chloride channel, the Na⁺-K⁺-2Cl⁻ (NKCC1) co-transporter encoded by *slc12a1* and *-a2*, and Ca²⁺ cation channels, among others[79–81]. AMPK also negatively regulates the CFTR and Cl⁻ secretion, and activation of AMPK with metformin inhibits CFTR secretion and reduces cyst growth[82–85]. Although the roles of other ion transporters in ADPKD have not been specifically addressed, alterations in the expression of any ion transporter that results in changes in ion concentrations in the cyst lumen could alter cyst development. In this study, we found that loss of *Fnip1* significantly alters the expression of numerous genes encoding cation and anion transporters; of the 206 genes down-regulated following disruption of *Fnip1*, we found the highest enrichment for genes associated with sodium-independent ion transport, organic ion transport, and anion transmembrane transport. These results suggest that one of

the functions of Fnip1 is to control ion transport, perhaps through AMPK activation, which could play a role in the development of PKD following disruption of *Fnip1*.

More recently, the roles of inflammatory cell infiltration in the development of ADPKD have been investigated with compelling results. In particular, interstitial inflammation characteristic of ADPKD and has been shown to result in elevated levels of cytokines and chemokines in the renal cyst fluid of patients with ADPKD, which is thought to contribute to disease progression [86–88]. Alternatively activated “M2-like” anti-inflammatory kidney macrophages, which are uniquely situated in close apposition to endothelial cells and basement membrane, have been shown to promote cyst growth in ADPKD by driving proliferation and fibrosis in the cystic epithelium, in part by induction of complement components including C3, TGF- β , and connective tissue growth factor (CTGF) [54, 89, 90]. Classically activated “M1” pro-inflammatory macrophages also contribute to epithelial cell damage by producing ROS and pro-inflammatory cytokines. Importantly, depletion of macrophages was shown to inhibit epithelial cell proliferation and cyst growth and improve renal function [54, 91]. In addition, PKD susceptible mice switched into a germfree environment fail to form cystic kidneys [92]. These results suggest that immune cell infiltration can play a unique and important role in the pathogenesis of PKD by producing pro-inflammatory mediators in response to tissue damage. Our results suggest that disruption of *Fnip1* alone results in increased kidney inflammation, specifically in the regions surrounding cysts. By IHC, we see enrichment of F4/80⁺ macrophages immediately surrounding cysts, and CD3⁺ T cells in similar regions. Using RNAseq and quantitative PCR, we found significant enrichment for genes involved in immune responses, including genes encoding complement components, Toll-like and NOD-like receptors, Fc-receptors, and S100 pro-inflammatory proteins. By flow cytometry, we found significant enrichment in the representation of myeloid cells in *Fnip1*^{-/-} kidneys. These results suggest that Fnip1 may normally suppress immune cell infiltration into the kidney parenchyma, which may function to limit inflammation and renal epithelial cell activation.

We also found that disruption of *Fnip1* potently synergizes with *Tsc1* loss to hyperactivate mTORC1 in otherwise normal renal tissue. This result further fuels the confusion as to whether the Fnip1/Fnip2/Folliculin complex is important for activating or inhibiting mTOR. Using siRNA knockdown approaches in human cell lines, two groups have presented evidence that Folliculin/Fnip recruits mTOR to the lysosome, where it is activated in response to amino acid stimulation [24, 25]. The conclusion made from these studies was that the Flcn/Fnip complex is necessary for GTP/GDP exchange in order to activate the Rag GTPases and to permit mTOR recruitment to the lysosome for activation. However, our data shows that loss of Fnip1 in kidney tissue results in increased activation of mTOR, and that loss of *Fnip1* synergizes with loss of *Tsc1* to further hyperactivate mTOR and greatly accelerate the development of PKD. Hasumi et al. found that kidney specific disruption of both *Fnip1* and *Fnip2* together using cadherin16-Cre (*CDH16*-Cre) resulted in severe PKD (50% survival around 21 days) characterized by increased activation of mTORC1 and PGC1 α . These results indicate that there is considerable functional compensation for the absence of Fnip1 by Fnip2 (and visa versa) either because their molecular functions are identical, or because disruption of *Fnip1* and *Fnip2* potently synergize to cause PKD due to activation of unique but cooperating pathways. Interestingly, although cyst formation was not observed in single *Fnip1*^{fl/fl} *CDH16*-Cre or *Fnip2*^{fl/fl} *CDH16*-Cre kidneys, the authors did find increased kidney/body weight and small cyst formation in *Fnip1*^{fl/fl} *Fnip2*^{fl/+} *CDH16*-Cre kidneys (31). The differences between our study and Hasumi et al may reflect differences in genetic background, or the use of kidney specific disruption of *Fnip1* by Hasumi et al versus constitutive disruption of *Fnip1* in our study. These results collectively suggest that Fnip1 may normally function in renal epithelial cells to limit activation of mTOR in this context. One potential model for how Fnip1 loss and *Tsc1* loss may

synergize to hyperactivate mTORC1, is that loss of Fnip1/Fnip2/Fln may result in increased recruitment of mTOR to the lysosome where it can be activated by Rheb, which is negatively regulated by TSC1. Consistent with this model, we also find that *Fnip1*^{-/-} skeletal muscle tissue [12] and pre-B cells [18] also exhibit hyperactivation of mTOR, and another laboratory has shown that AMPK via interaction with Axin and LKB1, is tethered with Fnip1/Fln at the lysosomal surface in response to low glucose, where it displaces mTORC1 [93]. Loss of Fnip1/Fln is predicted to inhibit AMPK recruitment and activation at the lysosome and facilitate mTORC1 recruitment and activation. Indeed, we find decreased AMPK activation and increased mTORC1 activation in *Fnip1* null renal tissue.

A major question is how Fnip1 controls so many molecular programs that, when dysregulated, may contribute to the development of PKD. One potential model is that Fnip1 controls the differentiation state of renal epithelial cells [94]. For example, it has been shown that renal gene expression differs considerably before and after postnatal day 13, when cell gene expression shifts abruptly from predominately proliferative to expression of genes also involved in cell polarity, extracellular matrix composition, and inflammation [95]. Perhaps loss of Fnip1 inhibits renal epithelial cells from adopting a more mature cell fate, thus altering their response to injury or mTOR activation, thus promoting cystogenesis. Consistent with this model, loss of Fnip1 inhibits differentiation of B lymphocytes [18, 96], invariant NK T cells [97], and embryonic stem cells [98], indicating that Fnip1 is linked to cellular differentiation in some cellular contexts.

Supporting information

S1 Fig. Disruption of Fnip1 results in increased mTORC1 signaling and decreased AMPK signaling in kidney cortical tissue. (A) Shown is quantitation of immunoblots in Fig 2A using densitometry followed by ImageJ analyses. * = p<0.05 (B) Immunoblots showing expression of Fnip1, Fnip2, and Folliculin protein in *Fnip1*^{-/-} and WT mice. Each lane represents 3 individual mice of the indicated genotype.
(TIFF)

S2 Fig. Electron microscopy on kidney tissue from *Fnip1* null and wildtype mice. Kidney tissue from 3 wildtype and 3 *Fnip1*^{-/-} mice were submitted for transmission EM. (A) Shown is a representative image of renal tubular epithelial cells. (B) Percent mitochondrial area is shown. Differences were not statistically significant.
(TIFF)

S3 Fig. Model of Fnip1 functions in kidney. (A) Proposed regulation of AMPK and mTOR by Fnip1. Fnip1 regulates the abilities of LKB1 and/or CamKK to activate AMPK. Fnip1 may regulate the localization activation of mTOR at the lysosome. (B) Model for Fnip1 functions in renal tissue. A number of cellular and molecular events have been linked to increased propensity to develop PKD. Shown of a proposed model for how loss of *Fnip1* could lead to the development of renal cysts.
(TIFF)

S4 Fig. Disruption of Fnip1 results in increased mTORC1 and increased Erk signaling in kidney cortical tissue. Shown is quantitation of immunoblots in Figs 7E and 8D using densitometry followed by ImageJ analyses. Significant P-values are shown.
(TIFF)

S1 Table. Metabolites significantly different between *Fnip1* null and wildtype kidney tissue as measured by liquid chromatography mass spectrometry (LC-MS/MS). Data were

analyzed using Metaboanalyst 3.0.
(TIFF)

S2 Table. Selected genes differentially expressed between *Fnip1* null and wildtype kidney tissue, as determined by RNAseq analyses.
(TIFF)

S3 Table. Ingenuity Upstream Regulator analyses showing disruption of *Fnip1* results in increased representation of specific transcriptional target genes.
(TIFF)

S4 Table. Oligonucleotide sequences used for quantitative PCR.
(TIFF)

Acknowledgments

We thank Winnie Kwong, Katy Cui, Monet Sklaroff for assistance with the mouse colony and genotyping; Brian Johnson from the UW Histology and Imaging Core for assistance with immunohistochemistry; and Ryan Basom with assistance with RNAseq analyses.

Author Contributions

Conceptualization: Ryan Centini, Brian M. Iritani.

Data curation: Ryan Centini, Mark Tsang, Terri Iwata, Heon Park, Jeffrey Delrow, Daciana Margineantu, Brandon M. Iritani, Haiwei Gu, H. Denny Liggitt, Janella Kang, Lim Kang, Daniel Raftery, Brian M. Iritani.

Formal analysis: Ryan Centini, Mark Tsang, Terri Iwata, Jeffrey Delrow, Daciana Margineantu, Brandon M. Iritani, Haiwei Gu, H. Denny Liggitt, Brian M. Iritani.

Funding acquisition: Brian M. Iritani.

Investigation: Ryan Centini, Terri Iwata, Heon Park, Daciana Margineantu, Brandon M. Iritani, Haiwei Gu, H. Denny Liggitt, Janella Kang, Lim Kang, Brian M. Iritani.

Methodology: Ryan Centini, Terri Iwata, Daciana Margineantu, David M. Hockenbery, Daniel Raftery, Brian M. Iritani.

Project administration: Ryan Centini, Brian M. Iritani.

Resources: Lim Kang, Brian M. Iritani.

Software: Jeffrey Delrow, Daniel Raftery.

Supervision: David M. Hockenbery, Daniel Raftery, Brian M. Iritani.

Validation: Ryan Centini, Terri Iwata, Brian M. Iritani.

Visualization: Ryan Centini, David M. Hockenbery, Brian M. Iritani.

Writing – original draft: Ryan Centini, Brian M. Iritani.

Writing – review & editing: Ryan Centini, Terri Iwata, Heon Park, David M. Hockenbery, Daniel Raftery, Brian M. Iritani.

References

1. Schmidt LS, Linehan WM. Molecular genetics and clinical features of Birt-Hogg-Dube syndrome. *Nat Rev Urol.* 2015; 12(10):558–69. <https://doi.org/10.1038/nrurol.2015.206> PMID: 26334087

2. Pavlovich CP, Walther MM, Eyler RA, Hewitt SM, Zbar B, Linehan WM, et al. Renal tumors in the Birt-Hogg-Dube syndrome. *Am J Surg Pathol*. 2002; 26(12):1542–52. PMID: [12459621](#).
3. Nickerson ML, Warren MB, Toro JR, Matrosova V, Glenn G, Turner ML, et al. Mutations in a novel gene lead to kidney tumors, lung wall defects, and benign tumors of the hair follicle in patients with the Birt-Hogg-Dube syndrome. *Cancer Cell*. 2002; 2(2):157–64. PMID: [12204536](#).
4. Baba M, Hong SB, Sharma N, Warren MB, Nickerson ML, Iwamatsu A, et al. Folliculin encoded by the BHD gene interacts with a binding protein, FNIP1, and AMPK, and is involved in AMPK and mTOR signaling. *Proc Natl Acad Sci U S A*. 2006; 103(42):15552–7. <https://doi.org/10.1073/pnas.0603781103> PMID: [17028174](#)
5. Hasumi H, Baba M, Hong SB, Hasumi Y, Huang Y, Yao M, et al. Identification and characterization of a novel folliculin-interacting protein FNIP2. *Gene*. 2008; 415(1–2):60–7. <https://doi.org/10.1016/j.gene.2008.02.022> PMID: [18403135](#)
6. Takagi Y, Kobayashi T, Shiono M, Wang L, Piao X, Sun G, et al. Interaction of folliculin (Birt-Hogg-Dube gene product) with a novel Fnip1-like (FnipL/Fnip2) protein. *Oncogene*. 2008; 27(40):5339–47. <https://doi.org/10.1038/onc.2008.261> PMID: [18663353](#).
7. Hardie DG, Schaffer BE, Brunet A. AMPK: An Energy-Sensing Pathway with Multiple Inputs and Outputs. *Trends Cell Biol*. 2016; 26(3):190–201. <https://doi.org/10.1016/j.tcb.2015.10.013> PMID: [26616193](#).
8. Fogarty S, Hawley SA, Green KA, Saner N, Mustard KJ, Hardie DG. Calmodulin-dependent protein kinase kinase-beta activates AMPK without forming a stable complex: synergistic effects of Ca²⁺ and AMP. *Biochem J*. 2010; 426(1):109–18. <https://doi.org/10.1042/BJ20091372> PMID: [19958286](#)
9. Gwinn DM, Shackelford DB, Egan DF, Mihaylova MM, Mery A, Vasquez DS, et al. AMPK phosphorylation of raptor mediates a metabolic checkpoint. *Mol Cell*. 2008; 30(2):214–26. <https://doi.org/10.1016/j.molcel.2008.03.003> PMID: [18439900](#)
10. Inoki K, Zhu T, Guan KL. TSC2 mediates cellular energy response to control cell growth and survival. *Cell*. 2003; 115(5):577–90. PMID: [14651849](#).
11. Yan M, Audet-Walsh E, Manteghi S, Dufour CR, Walker B, Baba M, et al. Chronic AMPK activation via loss of FLCN induces functional beige adipose tissue through PGC-1alpha/ERRalpha. *Genes Dev*. 2016; 30(9):1034–46. <https://doi.org/10.1101/gad.281410.116> PMID: [27151976](#)
12. Reyes NL, Banks GB, Tsang M, Margineantu D, Gu H, Djukovic D, et al. Fnip1 regulates skeletal muscle fiber type specification, fatigue resistance, and susceptibility to muscular dystrophy. *Proc Natl Acad Sci U S A*. 2015; 112(2):424–9. <https://doi.org/10.1073/pnas.1413021112> PMID: [25548157](#)
13. Khabibullin D, Medvetz DA, Pinilla M, Hariharan V, Li C, Hergueter A, et al. Folliculin regulates cell-cell adhesion, AMPK, and mTORC1 in a cell-type-specific manner in lung-derived cells. *Physiol Rep*. 2014; 2(8). <https://doi.org/10.14814/phy2.12107> PMID: [25121506](#)
14. Goncharova EA, Goncharov DA, James ML, Atochina-Vasserman EN, Stepanova V, Hong SB, et al. Folliculin controls lung alveolar enlargement and epithelial cell survival through E-cadherin, LKB1, and AMPK. *Cell Rep*. 2014; 7(2):412–23. <https://doi.org/10.1016/j.celrep.2014.03.025> PMID: [24726356](#)
15. Siggs OM, Stockenhuber A, Deobagkar-Lele M, Bull KR, Crockford TL, Kingston BL, et al. Mutation of Fnip1 is associated with B-cell deficiency, cardiomyopathy, and elevated AMPK activity. *Proc Natl Acad Sci U S A*. 2016; 113(26):E3706–15. <https://doi.org/10.1073/pnas.1607592113> PMID: [27303042](#)
16. Yan M, Gingras MC, Dunlop EA, Nouet Y, Dupuy F, Jalali Z, et al. The tumor suppressor folliculin regulates AMPK-dependent metabolic transformation. *J Clin Invest*. 2014; 124(6):2640–50. <https://doi.org/10.1172/JCI71749> PMID: [24762438](#)
17. Hasumi H, Baba M, Hasumi Y, Huang Y, Oh H, Hughes RM, et al. Regulation of mitochondrial oxidative metabolism by tumor suppressor FLCN. *J Natl Cancer Inst*. 2012; 104(22):1750–64. <https://doi.org/10.1093/jnci/djs418> PMID: [23150719](#)
18. Park H, Staehling K, Tsang M, Appleby MW, Brunkow ME, Margineantu D, et al. Disruption of Fnip1 reveals a metabolic checkpoint controlling B lymphocyte development. *Immunity*. 2012; 36(5):769–81. <https://doi.org/10.1016/j.immuni.2012.02.019> PMID: [22608497](#)
19. Klomp JA, Petillo D, Niemi NM, Dykema KJ, Chen J, Yang XJ, et al. Birt-Hogg-Dube renal tumors are genetically distinct from other renal neoplasias and are associated with up-regulation of mitochondrial gene expression. *BMC Med Genomics*. 2010; 3:59. <https://doi.org/10.1186/1755-8794-3-59> PMID: [21162720](#)
20. Possik E, Jalali Z, Nouet Y, Yan M, Gingras MC, Schmeisser K, et al. Folliculin regulates ampk-dependent autophagy and metabolic stress survival. *PLoS Genet*. 2014; 10(4):e1004273. <https://doi.org/10.1371/journal.pgen.1004273> PMID: [24763318](#)
21. Bastola P, Stratton Y, Kellner E, Mikhaylova O, Yi Y, Sartor MA, et al. Folliculin contributes to VHL tumor suppressing activity in renal cancer through regulation of autophagy. *PLoS One*. 2013; 8(7): e70030. <https://doi.org/10.1371/journal.pone.0070030> PMID: [23922894](#)

22. Hasumi Y, Baba M, Hasumi H, Huang Y, Lang M, Reindorf R, et al. Folliculin (Flcn) inactivation leads to murine cardiac hypertrophy through mTORC1 deregulation. *Hum Mol Genet.* 2014; 23(21):5706–19. <https://doi.org/10.1093/hmg/ddu286> PMID: 24908670
23. Hasumi Y, Baba M, Ajima R, Hasumi H, Valera VA, Klein ME, et al. Homozygous loss of BHD causes early embryonic lethality and kidney tumor development with activation of mTORC1 and mTORC2. *Proc Natl Acad Sci U S A.* 2009; 106(44):18722–7. <https://doi.org/10.1073/pnas.0908853106> PMID: 19850877
24. Petit CS, Roczniak-Ferguson A, Ferguson SM. Recruitment of folliculin to lysosomes supports the amino acid-dependent activation of Rag GTPases. *J Cell Biol.* 2013; 202(7):1107–22. <https://doi.org/10.1083/jcb.201307084> PMID: 24081491
25. Tsun ZY, Bar-Peled L, Chantranupong L, Zoncu R, Wang T, Kim C, et al. The folliculin tumor suppressor is a GAP for the RagC/D GTPases that signal amino acid levels to mTORC1. *Mol Cell.* 2013; 52(4):495–505. <https://doi.org/10.1016/j.molcel.2013.09.016> PMID: 24095279
26. Hartman TR, Nicolas E, Klein-Szanto A, Al-Saleem T, Cash TP, Simon MC, et al. The role of the Birt-Hogg-Dube protein in mTOR activation and renal tumorigenesis. *Oncogene.* 2009; 28(13):1594–604. <https://doi.org/10.1038/onc.2009.14> PMID: 19234517
27. Hudon V, Sabourin S, Dydensborg AB, Kottis V, Ghazi A, Paquet M, et al. Renal tumour suppressor function of the Birt-Hogg-Dube syndrome gene product folliculin. *J Med Genet.* 2010; 47(3):182–9. <https://doi.org/10.1136/jmg.2009.072009> PMID: 19843504.
28. Chen J, Futami K, Petillo D, Peng J, Wang P, Knol J, et al. Deficiency of FLCN in mouse kidney led to development of polycystic kidneys and renal neoplasia. *PLoS One.* 2008; 3(10):e3581. <https://doi.org/10.1371/journal.pone.0003581> PMID: 18974783
29. Baba M, Furihata M, Hong SB, Tessarollo L, Haines DC, Southon E, et al. Kidney-targeted Birt-Hogg-Dube gene inactivation in a mouse model: Erk1/2 and Akt-mTOR activation, cell hyperproliferation, and polycystic kidneys. *J Natl Cancer Inst.* 2008; 100(2):140–54. <https://doi.org/10.1093/jnci/djm288> PMID: 18182616
30. Chen J, Huang D, Rubera I, Futami K, Wang P, Zickert P, et al. Disruption of tubular Flcn expression as a mouse model for renal tumor induction. *Kidney Int.* 2015; 88(5):1057–69. <https://doi.org/10.1038/ki.2015.177> PMID: 26083655.
31. Hasumi H, Baba M, Hasumi Y, Lang M, Huang Y, Oh HF, et al. Folliculin-interacting proteins Fnip1 and Fnip2 play critical roles in kidney tumor suppression in cooperation with Flcn. *Proc Natl Acad Sci U S A.* 2015; 112(13):E1624–31. <https://doi.org/10.1073/pnas.1419502112> PMID: 25775561
32. Hobeika E, Thiemann S, Storch B, Jumaa H, Nielsen PJ, Pelanda R, et al. Testing gene function early in the B cell lineage in mb1-cre mice. *Proc Natl Acad Sci U S A.* 2006; 103(37):13789–94. <https://doi.org/10.1073/pnas.0605944103> PMID: 16940357
33. Kwiatkowski DJ, Zhang H, Bandura JL, Heiberger KM, Glogauer M, el-Hashemite N, et al. A mouse model of TSC1 reveals sex-dependent lethality from liver hemangiomas, and up-regulation of p70S6 kinase activity in Tsc1 null cells. *Hum Mol Genet.* 2002; 11(5):525–34. PMID: 11875047.
34. Iwata TN, Ramirez JA, Tsang M, Park H, Margineantu DH, Hockenbery DM, et al. Conditional Disruption of Raptor Reveals an Essential Role for mTORC1 in B Cell Development, Survival, and Metabolism. *J Immunol.* 2016; 197(6):2250–60. <https://doi.org/10.4049/jimmunol.1600492> PMID: 27521345
35. Park H, Staehling-Hampton K, Appleby MW, Brunkow ME, Habib T, Zhang Y, et al. A point mutation in the murine Hem1 gene reveals an essential role for Hematopoietic protein 1 in lymphopoiesis and innate immunity. *J Exp Med.* 2008; 205(12):2899–913. <https://doi.org/10.1084/jem.20080340> PMID: 19015308
36. Schmittgen TD, Livak KJ. Analyzing real-time PCR data by the comparative C(T) method. *Nat Protoc.* 2008; 3(6):1101–8. PMID: 18546601.
37. Zhu J, Djukovic D, Deng L, Gu H, Himmati F, Chiorean EG, et al. Colorectal cancer detection using targeted serum metabolic profiling. *J Proteome Res.* 2014; 13(9):4120–30. <https://doi.org/10.1021/pr500494u> PMID: 25126899
38. Sperber H, Mathieu J, Wang YL, Ferreccio A, Hesson J, Xu ZJ, et al. The metabolome regulates the epigenetic landscape during naive-to-primed human embryonic stem cell transition. *Nat Cell Biol.* 2015; 17(12):1523–35. <https://doi.org/10.1038/ncb3264> PMID: 26571212
39. Gu H, Zhang P, Zhu J, Raftery D. Globally Optimized Targeted Mass Spectrometry (GOT-MS): Reliable Metabolomics Analysis with Broad Coverage. *Anal Chem.* 2015; 87(24):12355–62. <https://doi.org/10.1021/acs.analchem.5b03812> PMID: 26579731
40. Gu H, Carroll PA, Du J, Zhu J, Neto FC, Eisenman RN, et al. Quantitative Method to Investigate the Balance between Metabolism and Proteome Biomass: Starting from Glycine. *Angew Chem Int Ed.* 2016; 55(50):15646–50.

41. Xia J, Wishart DS. Using MetaboAnalyst 3.0 for Comprehensive Metabolomics Data Analysis. *Curr Protoc Bioinformatics*. 2016; 55:14 0 1–0 91. <https://doi.org/10.1002/cpbi.11> PMID: 27603023.
42. Trapnell C, Pachter L, Salzberg SL. TopHat: discovering splice junctions with RNA-Seq. *Bioinformatics*. 2009; 25(9):1105–11. <https://doi.org/10.1093/bioinformatics/btp120> PMID: 19289445
43. Anders S, Pyl PT, Huber W. HTSeq—a Python framework to work with high-throughput sequencing data. *Bioinformatics*. 2015; 31(2):166–9. <https://doi.org/10.1093/bioinformatics/btu638> PMID: 25260700
44. Robinson MD, McCarthy DJ, Smyth GK. edgeR: a Bioconductor package for differential expression analysis of digital gene expression data. *Bioinformatics*. 2010; 26(1):139–40. <https://doi.org/10.1093/bioinformatics/btp616> PMID: 19910308
45. Reiner A, Yekutieli D, Benjamini Y. Identifying differentially expressed genes using false discovery rate controlling procedures. *Bioinformatics*. 2003; 19(3):368–75. PMID: 12584122.
46. Altobelli E, Angeletti PM, Latella G. Role of Urinary Biomarkers in the Diagnosis of Adenoma and Colorectal Cancer: A Systematic Review and Meta-Analysis. *J Cancer*. 2016; 7(14):1984–2004. <https://doi.org/10.7150/jca.16244> PMID: 27877214
47. Hsu WY, Chen CJ, Huang YC, Tsai FJ, Jeng LB, Lai CC. Urinary nucleosides as biomarkers of breast, colon, lung, and gastric cancer in Taiwanese. *PLoS One*. 2013; 8(12):e81701. <https://doi.org/10.1371/journal.pone.0081701> PMID: 24367489
48. Dominissini D, Nachtergaele S, Moshitch-Moshkovitz S, Peer E, Kol N, Ben-Haim MS, et al. The dynamic N(1)-methyladenosine methylome in eukaryotic messenger RNA. *Nature*. 2016; 530(7591):441–6. <https://doi.org/10.1038/nature16998> PMID: 26863196
49. Saxton RA, Sabatini DM. mTOR Signaling in Growth, Metabolism, and Disease. *Cell*. 2017; 169(2):361–71. <https://doi.org/10.1016/j.cell.2017.03.035> PMID: 28388417.
50. Kramer A, Green J, Pollard J Jr., Tugendreich S. Causal analysis approaches in Ingenuity Pathway Analysis. *Bioinformatics*. 2014; 30(4):523–30. <https://doi.org/10.1093/bioinformatics/btt703> PMID: 24336805
51. Trudel M, D'Agati V, Costantini F. C-myc as an inducer of polycystic kidney disease in transgenic mice. *Kidney Int*. 1991; 39(4):665–71. PMID: 1646908.
52. Sato Y, Yoshizato T, Shiraishi Y, Maekawa S, Okuno Y, Kamura T, et al. Integrated molecular analysis of clear-cell renal cell carcinoma. *Nat Genet*. 2013; 45(8):860–7. <https://doi.org/10.1038/ng.2699> PMID: 23797736.
53. Karihaloo A. Role of Inflammation in Polycystic Kidney Disease. In: Li X, editor. *Polycystic Kidney Disease*. Brisbane (AU)2015.
54. Karihaloo A, Koraihy F, Huen SC, Lee Y, Merrick D, Caplan MJ, et al. Macrophages promote cyst growth in polycystic kidney disease. *J Am Soc Nephrol*. 2011; 22(10):1809–14. <https://doi.org/10.1681/ASN.2011010084> PMID: 21921140
55. Harris PC, Torres VE. Genetic mechanisms and signaling pathways in autosomal dominant polycystic kidney disease. *J Clin Invest*. 2014; 124(6):2315–24. <https://doi.org/10.1172/JCI72272> PMID: 24892705
56. Boehlke C, Kotsis F, Patel V, Braeg S, Voelker H, Bredt S, et al. Primary cilia regulate mTORC1 activity and cell size through Lkb1. *Nat Cell Biol*. 2010; 12(11):1115–22. <https://doi.org/10.1038/ncb2117> PMID: 20972424
57. Chapin HC, Caplan MJ. The cell biology of polycystic kidney disease. *J Cell Biol*. 2010; 191(4):701–10. <https://doi.org/10.1083/jcb.201006173> PMID: 21079243
58. Seeger-Nukpezah T, Geynisman DM, Nikonova AS, Benzing T, Golemis EA. The hallmarks of cancer: relevance to the pathogenesis of polycystic kidney disease. *Nat Rev Nephrol*. 2015; 11(9):515–34. <https://doi.org/10.1038/nrneph.2015.46> PMID: 25870008.
59. Shillingford JM, Murcia NS, Larson CH, Low SH, Hedgepeth R, Brown N, et al. The mTOR pathway is regulated by polycystin-1, and its inhibition reverses renal cystogenesis in polycystic kidney disease. *Proc Natl Acad Sci U S A*. 2006; 103(14):5466–71. <https://doi.org/10.1073/pnas.0509694103> PMID: 16567633
60. Pema M, Drusian L, Chiaravalli M, Castelli M, Yao Q, Ricciardi S, et al. mTORC1-mediated inhibition of polycystin-1 expression drives renal cyst formation in tuberous sclerosis complex. *Nat Commun*. 2016; 7:10786. <https://doi.org/10.1038/ncomms10786> PMID: 26931735
61. Mostov KE. mTOR is out of control in polycystic kidney disease. *Proc Natl Acad Sci U S A*. 2006; 103(14):5247–8. <https://doi.org/10.1073/pnas.0601352103> PMID: 16567652
62. Hartman TR, Liu D, Zilfou JT, Robb V, Morrison T, Watnick T, et al. The tuberous sclerosis proteins regulate formation of the primary cilium via a rapamycin-insensitive and polycystin 1-independent pathway. *Hum Mol Genet*. 2009; 18(1):151–63. <https://doi.org/10.1093/hmg/ddn325> PMID: 18845692

63. Zhou J, Brugarolas J, Parada LF. Loss of Tsc1, but not Pten, in renal tubular cells causes polycystic kidney disease by activating mTORC1. *Hum Mol Genet.* 2009; 18(22):4428–41. <https://doi.org/10.1093/hmg/ddp398> PMID: 19692352.
64. Stine ZE, Walton ZE, Altman BJ, Hsieh AL, Dang CV. MYC, Metabolism, and Cancer. *Cancer Discov.* 2015; 5(10):1024–39. <https://doi.org/10.1158/2159-8290.CD-15-0507> PMID: 26382145
65. Riwanto M, Kapoor S, Rodriguez D, Edenhofer I, Segerer S, Wuthrich RP. Inhibition of Aerobic Glycolysis Attenuates Disease Progression in Polycystic Kidney Disease. *PLoS One.* 2016; 11(1):e0146654. <https://doi.org/10.1371/journal.pone.0146654> PMID: 26752072
66. Rowe I, Chiaravalli M, Mannella V, Ulisse V, Quilici G, Pema M, et al. Defective glucose metabolism in polycystic kidney disease identifies a new therapeutic strategy. *Nat Med.* 2013; 19(4):488–93. <https://doi.org/10.1038/nm.3092> PMID: 23524344
67. Han SH, Malaga-Dieguez L, Chinga F, Kang HM, Tao J, Reidy K, et al. Deletion of Lkb1 in Renal Tubular Epithelial Cells Leads to CKD by Altering Metabolism. *J Am Soc Nephrol.* 2016; 27(2):439–53. <https://doi.org/10.1681/ASN.2014121181> PMID: 26054542
68. Takiar V, Nishio S, Seo-Mayer P, King JD Jr., Li H, Zhang L, et al. Activating AMP-activated protein kinase (AMPK) slows renal cystogenesis. *Proc Natl Acad Sci U S A.* 2011; 108(6):2462–7. <https://doi.org/10.1073/pnas.1011498108> PMID: 21262823
69. Fragiadaki M, Lannoy M, Themanns M, Maurer B, Leonhard WN, Peters DJ, et al. STAT5 drives abnormal proliferation in autosomal dominant polycystic kidney disease. *Kidney Int.* 2017; 91(3):575–86. <https://doi.org/10.1016/j.kint.2016.10.039> PMID: 28104302.
70. Bhunia AK, Piontek K, Boletta A, Liu L, Qian F, Xu PN, et al. PKD1 induces p21(waf1) and regulation of the cell cycle via direct activation of the JAK-STAT signaling pathway in a process requiring PKD2. *Cell.* 2002; 109(2):157–68. PMID: 12007403.
71. Yamaguchi T, Reif GA, Calvet JP, Wallace DP. Sorafenib inhibits cAMP-dependent ERK activation, cell proliferation, and in vitro cyst growth of human ADPKD cyst epithelial cells. *Am J Physiol Renal Physiol.* 2010; 299(5):F944–51. <https://doi.org/10.1152/ajprenal.00387.2010> PMID: 20810616
72. Yamaguchi T, Pelling JC, Ramaswamy NT, Eppler JW, Wallace DP, Nagao S, et al. cAMP stimulates the in vitro proliferation of renal cyst epithelial cells by activating the extracellular signal-regulated kinase pathway. *Kidney Int.* 2000; 57(4):1460–71. <https://doi.org/10.1046/j.1523-1755.2000.00991.x> PMID: 10760082.
73. Buchholz B, Klanke B, Schley G, Bollag G, Tsai J, Kroening S, et al. The Raf kinase inhibitor PLX5568 slows cyst proliferation in rat polycystic kidney disease but promotes renal and hepatic fibrosis. *Nephrol Dial Transplant.* 2011; 26(11):3458–65. <https://doi.org/10.1093/ndt/gfr432> PMID: 21804086.
74. Lal M, Song X, Pluznick JL, Di Giovanni V, Merrick DM, Rosenblum ND, et al. Polycystin-1 C-terminal tail associates with beta-catenin and inhibits canonical Wnt signaling. *Hum Mol Genet.* 2008; 17(20):3105–17. <https://doi.org/10.1093/hmg/ddn208> PMID: 18632682
75. Happe H, Leonhard WN, van der Wal A, van de Water B, Lantinga-van Leeuwen IS, Breuning MH, et al. Toxic tubular injury in kidneys from Pkd1-deletion mice accelerates cystogenesis accompanied by dysregulated planar cell polarity and canonical Wnt signaling pathways. *Hum Mol Genet.* 2009; 18(14):2532–42. <https://doi.org/10.1093/hmg/ddp190> PMID: 19401297.
76. Song X, Di Giovanni V, He N, Wang K, Ingram A, Rosenblum ND, et al. Systems biology of autosomal dominant polycystic kidney disease (ADPKD): computational identification of gene expression pathways and integrated regulatory networks. *Hum Mol Genet.* 2009; 18(13):2328–43. <https://doi.org/10.1093/hmg/ddp165> PMID: 19346236.
77. Distefano G, Boca M, Rowe I, Wodarczyk C, Ma L, Piontek KB, et al. Polycystin-1 regulates extracellular signal-regulated kinase-dependent phosphorylation of tuberlin to control cell size through mTOR and its downstream effectors S6K and 4EBP1. *Mol Cell Biol.* 2009; 29(9):2359–71. <https://doi.org/10.1128/MCB.01259-08> PMID: 19255143
78. Grantham JJ. The etiology, pathogenesis, and treatment of autosomal dominant polycystic kidney disease: recent advances. *Am J Kidney Dis.* 1996; 28(6):788–803. PMID: 8957030.
79. Davidow CJ, Maser RL, Rome LA, Calvet JP, Grantham JJ. The cystic fibrosis transmembrane conductance regulator mediates transepithelial fluid secretion by human autosomal dominant polycystic kidney disease epithelium in vitro. *Kidney Int.* 1996; 50(1):208–18. PMID: 8807590.
80. Magenheimer BS, St John PL, Isom KS, Abrahamson DR, De Lisle RC, Wallace DP, et al. Early embryonic renal tubules of wild-type and polycystic kidney disease kidneys respond to cAMP stimulation with cystic fibrosis transmembrane conductance regulator/Na(+),K(+),2Cl(-) Co-transporter-dependent cystic dilation. *J Am Soc Nephrol.* 2006; 17(12):3424–37. <https://doi.org/10.1681/ASN.2006030295> PMID: 17108316.
81. Montesano R, Ghzili H, Carrozzino F, Rossier BC, Feraille E. cAMP-dependent chloride secretion mediates tubule enlargement and cyst formation by cultured mammalian collecting duct cells. *Am J*

- Physiol Renal Physiol. 2009; 296(2):F446–57. <https://doi.org/10.1152/ajprenal.90415.2008> PMID: 19052103.
82. Hallows KR, Raghuram V, Kemp BE, Witters LA, Foskett JK. Inhibition of cystic fibrosis transmembrane conductance regulator by novel interaction with the metabolic sensor AMP-activated protein kinase. *J Clin Invest*. 2000; 105(12):1711–21. <https://doi.org/10.1172/JCI9622> PMID: 10862786
 83. Hallows KR, McCane JE, Kemp BE, Witters LA, Foskett JK. Regulation of channel gating by AMP-activated protein kinase modulates cystic fibrosis transmembrane conductance regulator activity in lung submucosal cells. *J Biol Chem*. 2003; 278(2):998–1004. <https://doi.org/10.1074/jbc.M210621200> PMID: 12427743.
 84. King JD Jr., Fitch AC, Lee JK, McCane JE, Mak DO, Foskett JK, et al. AMP-activated protein kinase phosphorylation of the R domain inhibits PKA stimulation of CFTR. *Am J Physiol Cell Physiol*. 2009; 297(1):C94–101. <https://doi.org/10.1152/ajpcell.00677.2008> PMID: 19419994
 85. Kongsuphol P, Hieke B, Ousingsawat J, Almaca J, Viollet B, Schreiber R, et al. Regulation of Cl(-) secretion by AMPK in vivo. *Pflugers Arch*. 2009; 457(5):1071–8. <https://doi.org/10.1007/s00424-008-0577-3> PMID: 18752001.
 86. Gardner KD Jr., Burnside JS, Elzinga LW, Locksley RM. Cytokines in fluids from polycystic kidneys. *Kidney Int*. 1991; 39(4):718–24. PMID: 2051729.
 87. Merta M, Tesar V, Zima T, Jirsa M, Rysava R, Zabka J. Cytokine profile in autosomal dominant polycystic kidney disease. *Biochem Mol Biol Int*. 1997; 41(3):619–24. PMID: 9090470.
 88. Cowley BD Jr., Ricardo SD, Nagao S, Diamond JR. Increased renal expression of monocyte chemoattractant protein-1 and osteopontin in ADPKD in rats. *Kidney Int*. 2001; 60(6):2087–96. <https://doi.org/10.1046/j.1523-1755.2001.00065.x> PMID: 11737583.
 89. Swenson-Fields KI, Vivian CJ, Salah SM, Peda JD, Davis BM, van Rooijen N, et al. Macrophages promote polycystic kidney disease progression. *Kidney Int*. 2013; 83(5):855–64. <https://doi.org/10.1038/ki.2012.446> PMID: 23423256
 90. Mrug M, Zhou J, Woo Y, Cui X, Szalai AJ, Novak J, et al. Overexpression of innate immune response genes in a model of recessive polycystic kidney disease. *Kidney Int*. 2008; 73(1):63–76. <https://doi.org/10.1038/sj.ki.5002627> PMID: 17960140.
 91. Anders HJ, Ryu M. Renal microenvironments and macrophage phenotypes determine progression or resolution of renal inflammation and fibrosis. *Kidney Int*. 2011; 80(9):915–25. <https://doi.org/10.1038/ki.2011.217> PMID: 21814171.
 92. Werder AA, Amos MA, Nielsen AH, Wolfe GH. Comparative effects of germfree and ambient environments on the development of cystic kidney disease in CFWwd mice. *J Lab Clin Med*. 1984; 103(3):399–407. PMID: 6699465.
 93. Zhang CS, Jiang B, Li M, Zhu M, Peng Y, Zhang YL, et al. The lysosomal v-ATPase-Ragulator complex is a common activator for AMPK and mTORC1, acting as a switch between catabolism and anabolism. *Cell Metab*. 2014; 20(3):526–40. <https://doi.org/10.1016/j.cmet.2014.06.014> PMID: 25002183.
 94. Calvet JP. Injury and development in polycystic kidney disease. *Curr Opin Nephrol Hypertens*. 1994; 3(3):340–8. PMID: 7922262.
 95. Piontek K, Menezes LF, Garcia-Gonzalez MA, Huso DL, Germino GG. A critical developmental switch defines the kinetics of kidney cyst formation after loss of Pkd1. *Nat Med*. 2007; 13(12):1490–5. <https://doi.org/10.1038/nm1675> PMID: 17965720
 96. Baba M, Keller JR, Sun HW, Resch W, Kuchen S, Suh HC, et al. The folliculin-FNIP1 pathway deleted in human Birt-Hogg-Dube syndrome is required for murine B-cell development. *Blood*. 2012; 120(6):1254–61. <https://doi.org/10.1182/blood-2012-02-410407> PMID: 22709692
 97. Park H, Tsang M, Iritani BM, Bevan MJ. Metabolic regulator Fnip1 is crucial for iNKT lymphocyte development. *Proc Natl Acad Sci U S A*. 2014; 111(19):7066–71. <https://doi.org/10.1073/pnas.1406473111> PMID: 24785297
 98. Betschinger J, Nichols J, Dietmann S, Corrin PD, Paddison PJ, Smith A. Exit from pluripotency is gated by intracellular redistribution of the bHLH transcription factor Tfe3. *Cell*. 2013; 153(2):335–47. <https://doi.org/10.1016/j.cell.2013.03.012> PMID: 23582324